

Understanding ecohydrological connectivity in savannas: a system dynamics modelling approach

Gretchen R. Miller,^{1*} Jessica M. Cable,² Alyson K. McDonald,³ Barbara Bond,⁴ Trenton E. Franz,⁵ Lixin Wang,^{5,6} Si Gou,¹ Anna P. Tyler,⁷ Chris B. Zou⁸ and Russell L. Scott⁹

¹ Department of Civil Engineering, Texas A&M University, College Station, TX, USA

² International Arctic Research Center, University of Alaska, Fairbanks, AK, USA

³ Department of Ecosystem Science and Management, Texas AgriLife Extension Service, Texas A&M University, Fort Stockton, TX, USA

⁴ Department of Forest Ecosystems and Society, Oregon State University, Corvallis, OR, USA

⁵ Department of Civil and Environmental Engineering, Princeton University, Princeton, NJ, USA

⁶ School of Civil and Environmental Engineering, University of New South Wales, Sydney, NSW, Australia

⁷ Department of Ecology and Evolutionary Biology, University of Arizona, Tucson, AZ, USA

⁸ Department of Natural Resource, Ecology and Management, Oklahoma State University, Stillwater, OK, USA

⁹ Southwest Watershed Research Center, Agricultural Research Service, USDA, Tucson, AZ, USA

ABSTRACT

Ecohydrological connectivity is a system level property that results from the linkages in the networks of water transport through ecosystems, by which feedbacks and other emergent system behaviours may be generated. We created a system dynamics model that represents primary ecohydrological networks to examine how connectivity between ecosystem components impacts ecosystem processes. Here, we focused on the savanna ecosystems, although the analyses may be expanded to other ecosystem types in the future. To create the model, a set of differential equations representing ecohydrological processes was programmed into the dynamic solver Vensim. Stocks of water storage (e.g. atmospheric and soil moisture) were linked by flows [e.g. precipitation and evapotranspiration (ET)] that were in turn dynamically controlled by the amount of water stored. Precipitation was forced stochastically, and soil moisture and potential ET controlled actual ET. The model produced extended, probabilistic time series of stocks and flows, including precipitation, soil moisture, runoff, transpiration, and groundwater recharge. It was used to describe the behaviour of several previously studied savanna ecosystems in North America and Africa. The model successfully reproduced seasonal patterns of soil moisture dynamics and ET at the California site. It also demonstrated more complex, system level behaviours, such as multiyear persistence of drought and synergistic or antagonistic responses to disconnection of system components. Future improvements to the model will focus on capturing other important aspects of long-term system behaviour, such as changes in physiology or phenology, and spatial heterogeneity, such as the patchwork nature of savannas. Copyright © 2011 John Wiley & Sons, Ltd.

KEY WORDS cross-scale interactions; feedbacks; resilience; disturbance; system dynamics; soil moisture dynamics; evapotranspiration

Received 25 August 2010; Accepted 26 May 2011

INTRODUCTION

The ‘connectivity’ between components of an ecosystem influences overall system function and stability. The concept of ecosystem connectivity originated with studies in animal population dynamics in the 1970s, where it represents the ‘degree to which the landscape facilitates or impedes movement among resource patches’ (Tischendorf and Fahring, 2000). In other disciplines, connectivity has been defined and utilized inconsistently (Calabrese and Fagan, 2004), as it has been used to describe processes related to both structure and function of landscapes (Tischendorf and Fahring, 2000). We suggest that connectivity is a system level characteristic that describes networks of a medium or transport vectors, such as wind, water, and animals, which link patchworks of

resources or organisms. Connectivity essentially results from a network–patchwork association.

More recently, the concept of connectivity has been applied to physical (soil) and biological (plant) processes within and across ecosystems, specifically the exchange of matter and energy at multiple temporal and spatial scales (Peters *et al.*, 2006). Connectivity can occur in the vertical or horizontal plane and there may be a variety of connecting media. In semi-arid ecosystems, water is the primary medium of connectivity because it controls physical and biological processes across scales (Austin *et al.*, 2004; Wang *et al.*, 2009). Rates of movement and exchange of water depend upon the characteristics and connectivity of pathways, such as the soil–plant–atmosphere continuum (vertical connectivity), soil properties (both vertical and horizontal connectivity), and the distribution of plants on the landscape (horizontal connectivity), as shown in Figure 1.

Quantifying connectivity can be challenging, and evidence of connectivity is clear in some situations but

* Correspondence to: Gretchen R. Miller, Department of Civil Engineering, Texas A&M University, College Station, TX, USA.
E-mail: gmiller@civil.tamu.edu

MODELLING CONNECTIVITY IN SAVANNA ECOSYSTEMS

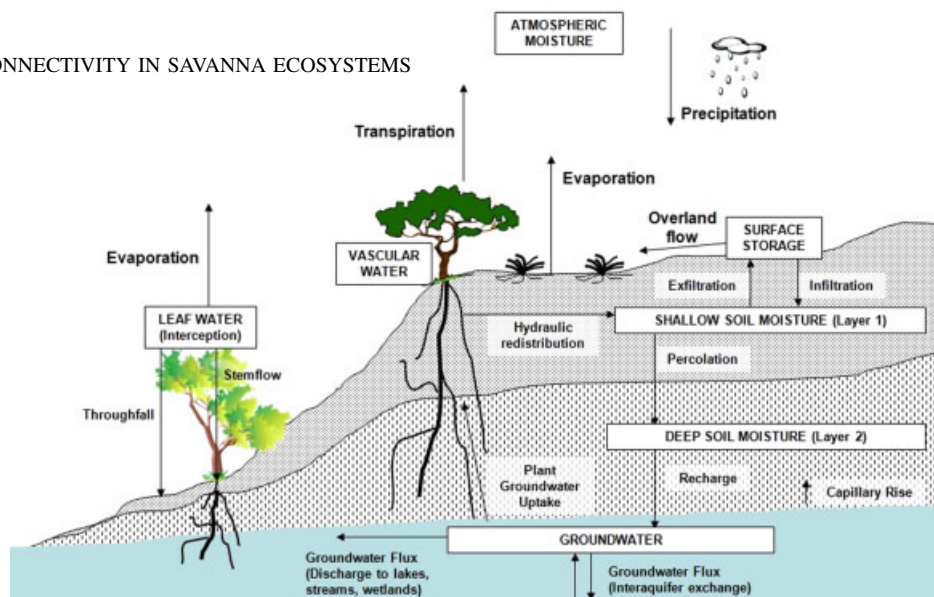


Figure 1. A conceptual diagram depicting the horizontal and vertical connectivity of an ecosystem with water as the primary medium. The pools between which the water is moving include different layers of soil, vegetation, and atmosphere. The vertical connections occur at several levels. The first is the upward movement of water via the soil–plant–atmosphere continuum (plant transpiration, evaporation from soil, and plant interception) or just the soil–atmosphere continuum (soil evaporation). The second is downward movement of water in the soil via infiltration of rainfall, water exfiltration, percolation, and recharge. The horizontal connections occur on the soil surface as overland flow and in subsurface layers as lateral flow.

only suggestive in others. Adding to the complexity, connectivity can be cyclic or unidirectional. Rainfall recycling from evapotranspiration (ET) is an example of cyclic connectivity, where the connection between water in the soil, plants, and the atmosphere results in water retention within the system (Richards and Caldwell, 1987; Sala *et al.*, 1989; Dawson and Ehleringer, 1991; Trenberth, 1999). A clear example of unidirectional connectivity is overland water flow, or run-on and runoff, where water moves downslope and redistributes to a different location, such as a depression or vegetated patch (Reid *et al.*, 1999; Dunkerley, 2002; Ludwig *et al.*, 2005), and transports with it soil nutrients in the form of litter or dissolved inorganic chemicals (Belnap *et al.*, 2005; Wang *et al.*, 2011).

Modelling connectivity at the ecosystem level is also a complex problem, largely due to cross-scale interactions (Peters *et al.*, 2008) and the ‘paradox of scale’ (Wilcox *et al.*, 2006), wherein organ-, organism-, or plot-level processes tend not to scale to the ecosystem level. This suggests that whole ecosystems behave differently—with regard to controls over water and carbon fluxes—than the sum of the individual parts (Osmond *et al.*, 2004). Thus, small-scale measurements are not likely to capture the connectivity occurring on different temporal and spatial scales. Time lags in plot- or leaf-level processes can create temporal discontinuities, while variations in micro-scale soil texture, interplant variability, and patchiness in soil microbial distributions can induce spatial differences. Essentially, by capturing spatial and/or temporal ‘snapshots’ of physical and biological activities via spot measurements, the connectivity between different ecosystem components is likely to be missed, and the network–patchwork dynamic of fluxes will not be

captured. This limits our ability to predict how broad changes in climate or land use may impact ecosystem processes (Tang and Bartlein, 2008).

A more robust understanding of ecosystem connectivity may contribute to predicting the effects of environmental change, from land use to climate change, on ecosystems. For example, there may be an optimum level and type of connectivity that creates resilience and stability in ecosystem function (Haydon, 2000; Sole and Montoya, 2001; Peters *et al.*, 2004). Loss or creation of connectivity could lead to state transition (Briske *et al.*, 2005). Widespread shrub encroachment into grasslands (Schlesinger *et al.*, 1990; Archer, 1994; Van Auken, 2000) is a significant example of a change in connectivity. The resulting fragmentation of grasslands causes a shift from a homogeneous to heterogeneous distribution of water and soil nutrients, whereby resources become concentrated around woody plants (‘islands of fertility’), leaving exposed soil in adjacent interspaces formerly occupied by grasses (Schlesinger *et al.*, 1990; Bhark and Small, 2003; Okin *et al.*, 2009; Ravi *et al.*, 2010). This ‘patchiness’ also drives spatial variation in soil and ecosystem processes, and can decouple ecosystem processes, such as plant production, from climate drivers, such as precipitation (Scott *et al.*, 2006).

Savanna ecosystems occur in semi-arid climates and are ecotones that have different plant functional types (shrubs, trees, and grasses), which create high spatial heterogeneity of woody canopy cover and have different rooting distributions (Wiegand *et al.*, 2006). Given this inherent patchiness, savanna ecosystems are ideal for exploring the network–patchwork dynamics of connectivity and studying the propensity of an ecosystem to shift from grass to shrub dominated. Additionally,

these ecosystems are useful for identifying thresholds of connectivity required to maintain a grassland component within the savanna ecosystem.

Various metrics to quantify and further describe spatial arrangement of patches have been developed to understand urbanization, desertification, organism dispersal, and changes in viable wildlife habitat (Calabrese and Fagan, 2004). Strongly connected systems are more likely to exhibit nonlinear spatial dynamics (Peters *et al.*, 2008), and feedbacks complicate interpretation and prediction of system behaviour. Rather than emphasizing the quality and quantity of connectivity, we suggest that system dynamics (SD) models can be employed to advance our understanding of nonlinear systems and their behaviours.

SD was borne out of feedback control systems developed during World War II (Forrester, 2007) and later expanded to aid in analyzing dynamic systems with complex feedbacks. More recently it has been applied to studies from various natural and agricultural environments, such as developing reservoir operation procedures (Ahmad and Simonovic, 2000), modelling soil salinization of irrigated croplands (Saysel and Barlas, 2001), and evaluating surface–groundwater interactions (Khan *et al.*, 2009). SD models efficiently produce major dynamic patterns such as exponential growth, thresholds, and other emergent system level behaviours (Khan *et al.*, 2009). While SD models are not appropriate for forecasting, they are a useful tool in validating system structure and understanding of processes and patterns (Saysel and Barlas, 2001).

An SD approach is especially appropriate for connectivity studies because it is able to eliminate the artificial separation of processes that is inherent to most models and that prevents feedbacks from being adequately studied. For instance, we know that atmospheric moisture is closely connected to other hydrological processes: it both controls and is controlled by precipitation and ET rates. However, it is not typically included as a state variable in modelling efforts, rather atmospheric moisture and precipitation are prescribed in a top-down fashion, using time series of weather data that cannot be influenced by internal system processes. Thus, ecological and hydrological models that resolve behaviours arising from land–atmosphere interactions, such as the influence of antecedent soil moisture on subsequent precipitation (D'Odorico and Porporato, 2004) are rare.

In this study, we ask, are there emergent behaviours of connected versus disconnected ecosystems and can these behaviours be quantified? We aimed to illuminate the properties and consequences of connectivity across several different savanna ecosystems varying in soil, climate, and vegetation composition. This was accomplished by creating a relatively simple SD model to explore how connectivity via water pathways might affect savanna ecohydrological responses, primarily ET flux, to environmental presses and pulses related to water availability, such as drought and declining groundwater levels. We constructed three ecosystem 'disturbance scenarios' to ask questions such as: How do water flows from differing

savannas behave in response to environmental presses and pulses and how is this related to connectivity? How does the degree and nature of ecohydrological connectivity impact land surface–atmosphere moisture interactions, such as rainfall recycling? Do the connections in savanna ecosystems create synergistic effects, such as buffering the system from drought or enhancing precipitation?

METHODS

Model development

We created the model itself using the simulation software package Vensim 5.8a (Ventana Systems Inc., Harvard, MA, USA). Vensim is designed to simultaneously solve a series of differential equations, each representing the change in material held within a stock and its depletion or replenishment by flow into and out of the stock (Ventana Systems, 2007a,b). Here, stocks represent the mass of water within a given reservoir in the natural environment, while the flows represent the fluxes of water. While this model was created on the full version of the software (Vensim DSS), it also runs on Vensim PLE, which is available freely to the academic community for use in education and research. The model formulation developed, including the equations used to calculate the stocks and the flows, is described in detail in the Appendix.

Model runs were conducted using a one-day time-step, with state variables reported at every interval. All stock (storage) terms were given in millimetres (to represent a 'column' of water over a unit area), and flow terms were given in millimetres per day. Throughout the model construction, certain assumptions and simplifications were made, in order to make the modelling effort tenable. These include (1) using monthly, site-based estimates of ET potential, rather than actual time series or process-driven predictions, such as vapor pressure deficit (VPD) dependent ET, (2) holding the phenology of woody vegetation constant and not including vegetation growth or dispersal, (3) using one, multilayered soil moisture 'bucket' for both the grassy and woody vegetation, instead of creating a patchwork soil system to separate understory and open area grass, and (4) that soil type and fraction of overstory coverage were homogeneous over a stand-scale area, as reflected by the use of eddy covariance data for model testing.

Site descriptions

Data from four savannas, which represent the wide range of characteristics found in these biomes, were compiled for use as modelling parameters (Table I, Figures 2 and 3). These systems range between sites in the Kenyan highlands, the Kalahari transect (KT) in southern Africa, a riparian area within the Sonoran Desert, and a California savanna. Each ecosystem is dominated by different species of shrubs and grasses. The following are brief descriptions of each site, along with

Table I. Model parameters for savanna sites used in this study.

Symbol	Definition	Units	Tshane	Pandamatenga	Kenya Red	Kenya Black	Arizona	California
τ	Mean time between rainfall events	day	TD	TD	TD	TD	TD	TD
α	Mean rainfall depth	mm	TD	TD	TD	TD	TD	TD
$S_{leaf,max}$	Interception	mm	1.2	2.3	0.5	0.75	1.0 ^a	1.2
$S_{atmos,sat}$	Precipitable water column	mm	TD	TD	TD	TD	TD	TD
f_r	Recycling factor	Percent	2	2	7	7	20	4
z_1	Soil 1 thickness	mm	800	795	500	500	400	250
z_2	Soil 2 thickness	mm	2000	50	500	1000	400	300
$S_{s1,max}$	Maximum soil water storage, layer 1	mm	368	350	232.5	250	152	135
$S_{s2,max}$	Maximum soil water storage, layer 2	mm	920	22	232.5	500	152	159
$S_{fc,s1}$	Field capacity, layer 1	- mm	0.093 34.2	0.095 33.25	0.66 153.5	0.78 195	0.46 69.9	0.70 94.5
$S_{fc,s2}$	Field capacity, layer 2	- mm	0.093 85.6	0.090 1.98	0.66 153.5	0.78 390	0.32 48.6	0.80 127.2
S_h	Hygroscopic point, layer 1	- mm	0.015 5.52	0.020 7.00	0.32 74.4	0.47 117.5	0.12 18.2	0.10 13.5
K_{s1}	Saturated hydraulic conductivity, layer 1	mm/day	16 000	14 000	450	50	1600	400
K_{s2}	Saturated hydraulic conductivity, layer 2	mm/day	6400	14 000	450	10	1000	400
f_{run}	Runoff coefficient	—	0.96 ^a	0.94 ^a	0.94 ^a	0.94 ^a	0.98	0.94
f_{se}	Fraction of E_{max} from soil evaporation	Percent	0.02 ^a	0.01 ^a	0.05	0.05	TD	TD (0.05–0.1)
$S_{g^*,s1}$	Point of incipient stress, grass, layer 1	- mm	0.040 14.7	0.085 29.8	0.48 111.6	0.62 155	0.20 30.4	0.45 60.75
$S_{w^*,s1}$	Point of incipient stress, woody, layer 1	- mm	0.078 28.7	0.085 29.8	0.48 111.6	0.62 155	0.28 42.6	0.43 58.1
$S_{w^*,s2}$	Point of incipient stress, woody, layer 2	- mm	0.078 71.8	0.085 1.87	0.48 111.6	0.62 310	0.24 36.5	0.48 76.3
$S_{gc,s1}$	Stomatal closure point, grass, layer 1	- mm	0.035 12.9	0.035 12.3	0.39 90.7	0.57 142.5	0.17 25.8	0.30 40.5
$S_{wc,s1}$	Stomatal closure point, woody, layer 1	- mm	0.036 13.2	0.037 13.0	0.36 83.7	0.52 130	0.20 30.4	0.26 35.1
$S_{wc,s2}$	Stomatal closure point, woody, layer 2	- mm	0.036 33.1	0.037 0.82	0.36 83.7	0.52 260	0.21 31.9	0.36 57.2
$E_{max,grass}$	Maximum ET, grass vegetation	mm/day	TD	TD	TD	TD	TD	TD
$E_{max,woody}$	Maximum ET, woody vegetation	mm/day	TD	TD	TD	TD	TD	TD
$f_{g,s1}$	Grass root fraction, soil layer 1	Fraction	1	1	1	1	1	1
$f_{g,s2}$	Grass root fraction, soil layer 2	Fraction	0	0	0	0	0	0
$f_{w,s1}$	Woody vegetation root fraction, soil layer 1	Fraction	0.8	0.9	0.7	0.8	0.21	0.34
$f_{w,s2}$	Woody vegetation root fraction, soil layer 2	Fraction	0.2	0.1	0.3	0.2	0.11	0.42
$f_{w,g}$	Woody vegetation root fraction, groundwater	Fraction	0	0	0	0	0.68	0.24

TD, time-dependent parameter shown in Figures 2 and 3. For soil saturation values, the values on the left indicate water saturation (e.g. saturation at the soil's hygroscopic point) while the values on the right is the total water stored (e.g. the 'height' of the water column in the soil at the hygroscopic point).

^a parameters unknown for sites and estimated based on information from other sites.

the methods used to collect the data and the duration of the monitoring conducted. Photographs of each site may be found in Figure 4.

California savanna. California's natural vegetation gently grades from grasslands near the very dry center of the state, through savannas on the moderately

dry foothills, to woodlands and montane forests as elevation and precipitation increase. The Tonzi Ranch site (38.4311 °N, 120.966 °W, 177 m above sea level) is a tree-grass savanna (Figure 4e), and the climate is semi-arid and Mediterranean. Mean annual precipitation (MAP) is approximately 560 mm, with rainfall primarily

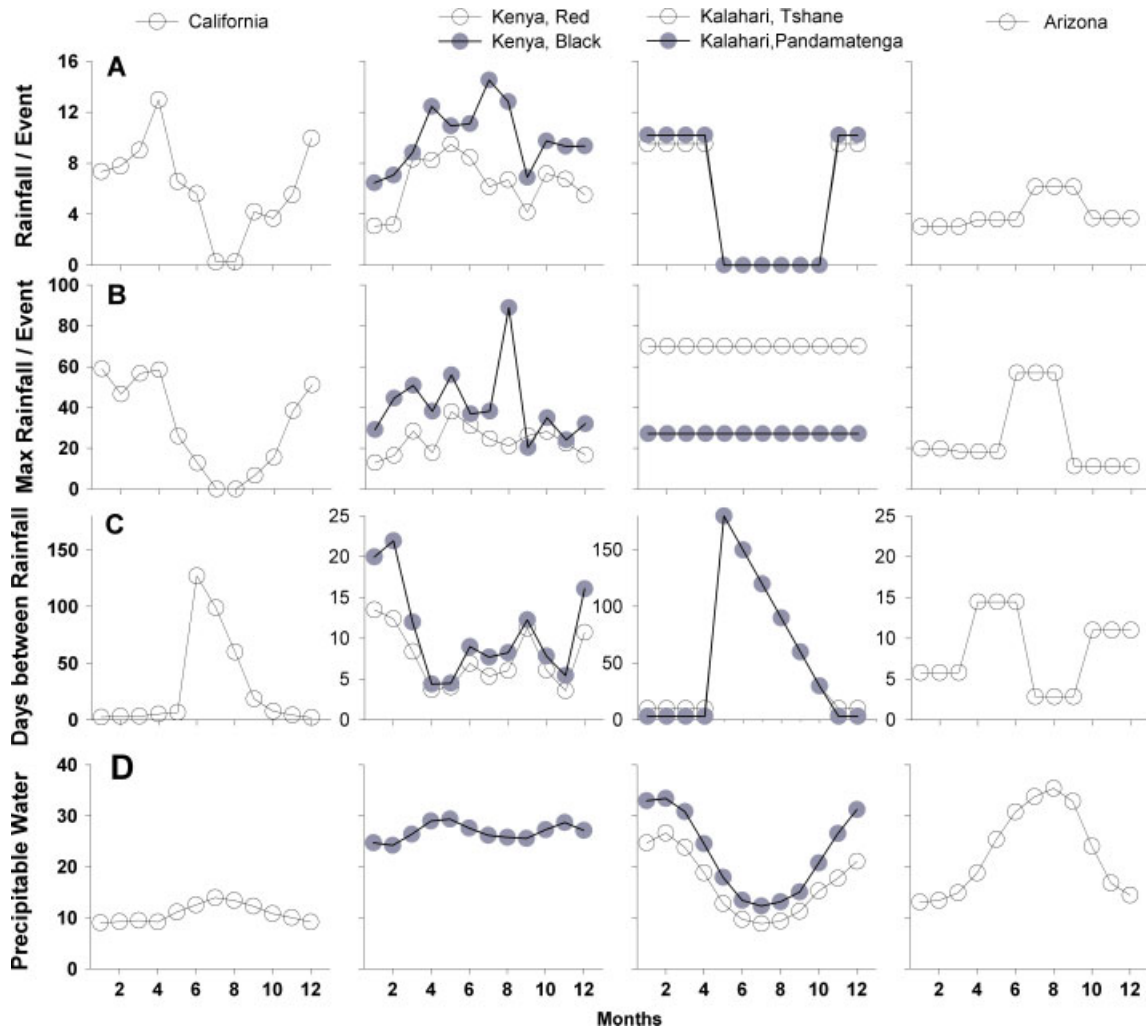


Figure 2. Plots of time-dependent rainfall parameters. (a) Average depth of rainfall per event, (b) maximum rainfall per event, (c) average time between rainfall events, and (d) average monthly precipitable water column. Values were calculated on a monthly basis for the Kenya Red Soil and Black Cotton sites (27 and 29 years available, respectively) and on a monthly to seasonal basis for California (7 years) and Arizona (5 years), as constrained by the records available.

confined to the wet season, from October to May (Baldocchi *et al.*, 2004). The overstorey covers approximately 45% of the landscape and is dominated by deciduous blue oaks (*Quercus douglassi*), with grey pines (*Pinus sabiniana*) scattered throughout. The understory consists of non-native herbs and grasses, including *Brachypodium distachyon*, *Bromus hordeaceus*, *Erodium cicutarium*, and *Hypochaeris glabra* (Baldocchi *et al.*, 2010). Data collection has occurred continuously since 2001; measurements include standard meteorological variables, soil moisture from both time-domain reflectometer and capacitance probes, and fluxes of carbon and water from eddy covariance. An ecohydrological, cross-comparison study reported soil, precipitation, and ET parameters for the site (Miller *et al.*, 2007). At the site, the depth to groundwater ranges from 7 to 12 m, depending on season and location. In 2007 and 2008, uptake of groundwater by the oak trees at the site resulted in an average of 76 mm of transpiration per year, 20% of total ET (Miller *et al.*, 2010).

Arizona savanna. The research site is a riparian shrubland (Figure 4f) located on an old alluvial terrace of the

San Pedro River in southeastern Arizona, near Sierra Vista (1200 m above sea level), where mean summer temperature is 26 °C and the climate is semi-arid with an MAP ~360 mm. Rainfall has a bimodal distribution throughout the year; 60% falls during the monsoon (June to September) and about 30% falls between December and March. The site is a medium dense shrub–grass ecosystem with a mix of velvet mesquite (*Prosopis velutina*) (1–4.5 m tall) and sacaton bunchgrass (*Sporobolus wrightii*). The mesquite shrubs vary in height; those between 1.5 and 3 m tall were categorized as medium-sized and those more than 3 m tall as large-sized. Depth to groundwater is estimated to be 6.5 m, making it accessible only to the medium- to large-size mesquites (Potts *et al.*, 2008). The primary microsites and their relative ground cover on the landscape are medium-sized mesquite (31.1%), large-sized mesquite (20.4%), bunchgrass (22.3%), open ground with litter (11.8%), open ground without litter (11.0%), and other types of ground cover (5.1%). Measurements include standard micrometeorological variables (precipitation, air temperature, soil moisture and temperature, relative humidity,

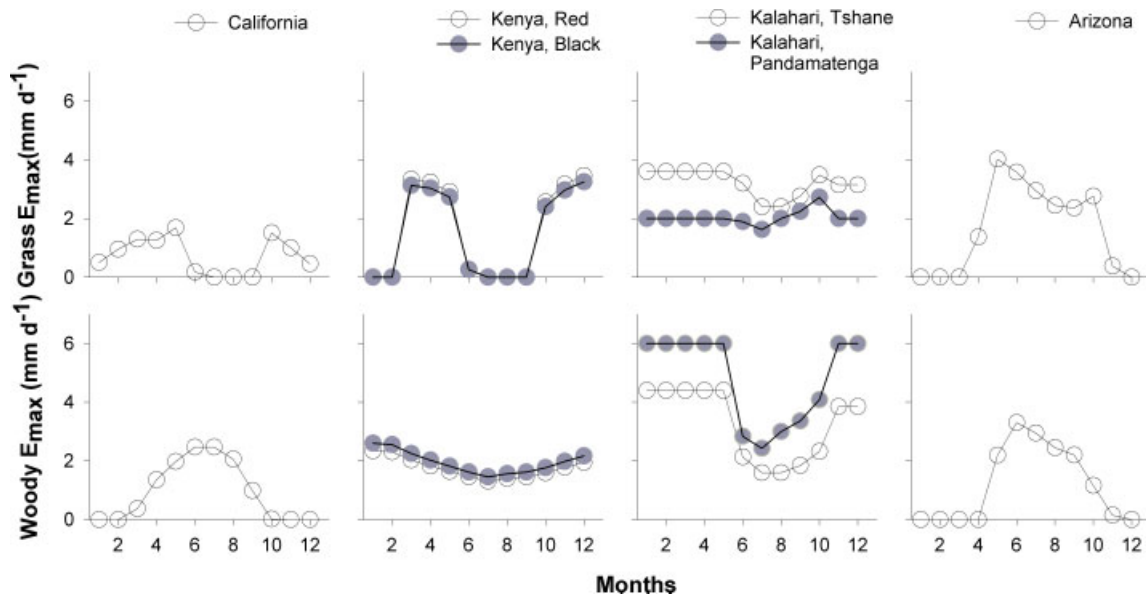


Figure 3. Plots of E_{max} as a function of time. The term E_{max} represents the theoretical maximum transpiration that would occur if the vegetation at a site had unlimited soil moisture available. In the model, it is divided into an $E_{max,grass}$ for grasses (a) and an $E_{max,woody}$ for woody vegetation (b). E_{max} is calculated within the program, using the inputs of potential evaporation (E_{pot}), fraction of woody canopy coverage (f_{canopy}), and a phenology indicator, which is equal to one when the vegetation type is active and zero after it has senesced.

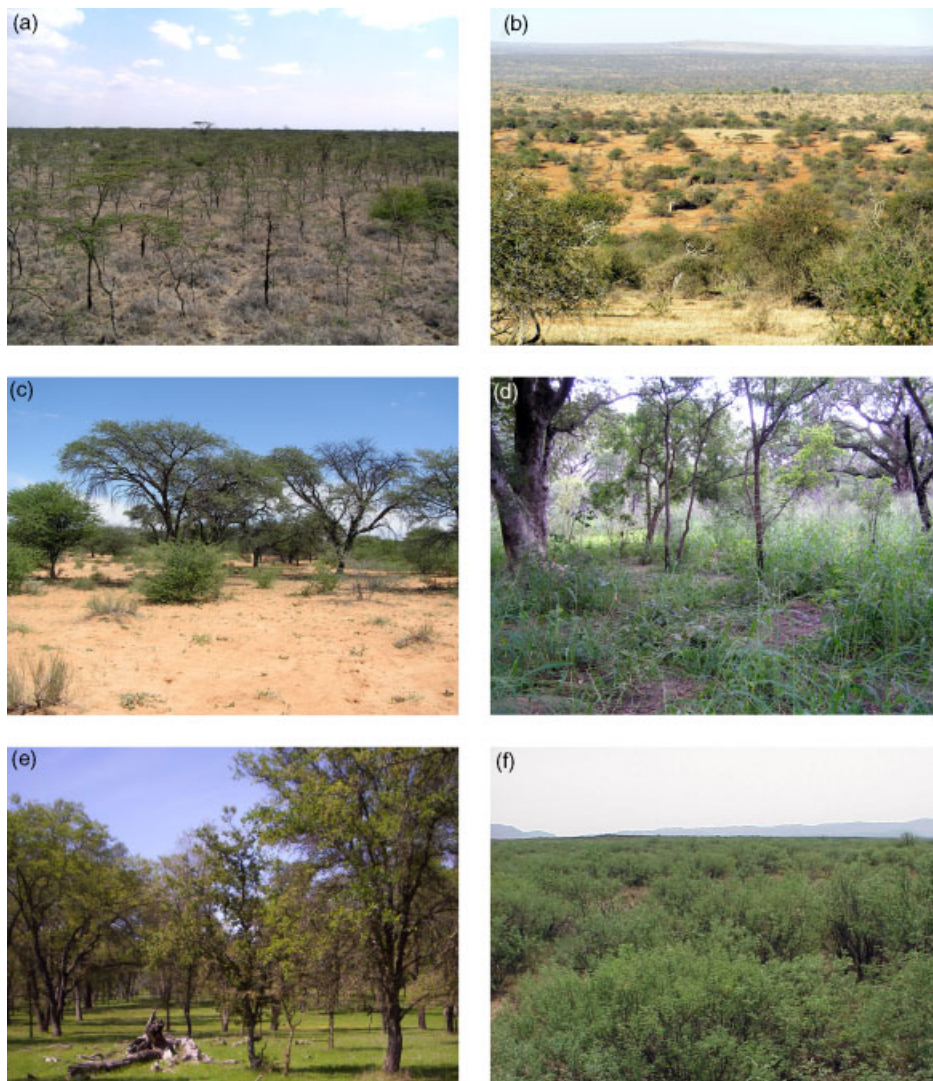


Figure 4. Photographs of each savanna site, from left to right, by row: (a) Kenya—Black Cotton soils, (b) Kenya—Red soils, (c) Kalahari—Tshane (dry), (d) Kalahari—Pandamatenga (wet), (e) California—Tonzi Ranch, and (f) Arizona—San Pedro River.

solar radiation), eddy covariance (ecosystem fluxes of CO₂ and H₂O vapor, LiCor 7500), soil respiration (LiCor 820), and leaf-level gas exchange (LiCor 6400, LiCor, Lincoln, NE, USA) (Scott *et al.*, 2006).

Kenya savannas. The central Kenya highlands are a classical tree-grass savanna that spans a large elevation and precipitation gradient (Franz *et al.*, 2010). The basin is composed of a variety of soil textures that leads to a heterogeneous mosaic of vegetation. The basin is situated at the equator so rainfall comes in two wet seasons, the long rains (March–May) and the short rains (October–December). While very little rainfall occurs during the hot dry season (January–February), the cold dry season (June–September) may produce additional rainfall. Two sites in the basin were chosen to compare the potential connections and feedbacks within the system. The first, referred to as the Kenya Black Cotton site (0.28°N, 36.87°E), is home to the Kenya Long-term Experimental Enclosure (KLEE) project (Young *et al.*, 1998) and receives ~520 mm MAP. Clay vertisol or ‘black cotton’ soils support a homogeneous woody canopy (Figure 4a) of *Acacia drepanolobium* (Young *et al.*, 1998). Understory vegetation is composed primarily of five perennial grass species *Pennisetum stramineum*, *Lintonia nutans*, *Themeda triandra*, *Pennisetum mezianum*, and *Brachiaria lachnanth* (Young *et al.*, 1998). From July to August 2009, a portable micrometeorological and eddy covariance tower (10 m) were placed at the site.

The second, called the Kenya Red Soil site (0.50°N, 36.92°E), is located on communal Maasai lands and receives ~465 mm MAP. The vegetation community on the sandy clay loam red soils is more diverse and variable (Figure 4b), with the dominant woody genus being *Acacia* (sp. *tortilis*, *mellifera*, *etbaica*, *seyal*, *nilotica*) and the herbaceous community comprised of various grasses from the genera *Cynodon*, *Pennisetum*, *Digitaria*, and *Sporobolus* (Young *et al.*, 1995). Beginning in 2006, we quantified soil properties (texture, porosity), and temporal (time domain reflectometry) and spatial patterns (electromagnetic induction) of soil moisture in the near surface (0–100 cm) (Franz *et al.*, 2011). A permanent micrometeorological and eddy covariance station (25 m) was installed in February 2010. Climate, soil, and vegetation parameters for the different study sites are summarized by Franz *et al.* (2010). No evidence for groundwater uptake has been found at either of these sites.

Kalahari savannas. The north–south transect of the Kalahari (known as the KT) in southern Africa is one of a set of International Geosphere–Biosphere Programme (IGBP) ‘megatransects’. Two sites (Tshane and Pandamatenga) along the KT were chosen to compare the hydrological connectivity under different climate conditions, with Tshane occurring at the dry end of the transect (~300 mm MAP) and Pandamatenga occurring at the wet end (~700 mm MAP). Rainfall at both sites is concentrated between November and April (wet season), and

the rest of time is dry season. The Tshane site (24.17°S, 21.89°E) is classified as open savanna dominated by *Acacia* species such as *Acacia luederitzii* Engl. and *Acacia mellifera* Benth., and grass species, such as *Eragrostis lehmanniana* and *Schmidtia pappophoroides* (Figure 4c). The Pandamatenga site (18.16°S, 25.50°E) is classified as woodland savanna dominated by tree species such as *Kirkia Africana* (Figure 4d). The common observed grass species are *Panicum maximum*, *Schmidtia pappophoroides* and *Pogonarihria squarrosa*. Most of the tree species in these systems are C₃ plants and grasses are C₄ plants. Soil properties such as porosity, field capacity, saturated hydraulic conductivity, as well as soil and litter carbon/nitrogen ratios were determined for these two sites from samples collected from the 2005 and 2006 wet seasons at both ‘tree’ (less than 10% of grass cover) and ‘grass’ microsites (Wang *et al.*, 2007). Direct rainfall measurements at the Kalahari sites are not available. We estimated the rainfall parameters (e.g., average rainfall depth and average rainfall frequency) based on values from similar savanna vegetation types and the parameters were validated with continuous field soil moisture measurements; for details please refer to Wang *et al.* (2009). No evidence for groundwater uptake has been found at either of these sites.

Model testing and sensitivity analysis

Site-specific parameter sets were implemented within the model, with each separate simulation representing one of six different savanna ecosystems. Both ‘stock’ and ‘flow’ values were recorded at daily and yearly intervals for a 10-year time-span, with special focus being placed on soil moisture, woody ET, grass ET, and total ET as the important ecohydrological response variables.

Two of these simulations, that from the California oak savanna and the Arizona riparian shrubland, were selected to test model response as compared to available ET and soil moisture data. To conduct these site-specific test, the simulation was forced with actual precipitation data (rather than randomly generated values), collected over the span of 4 years, 2005–2008 for California and 2004–2007 for Arizona. The model simulation for the California site was calibrated against the 2005 and 2007 data in order to achieve a better fit with the observed water balance data. This calibration was accomplished by altering the following uncertain parameters, within the range of reasonable values for the site: soil field capacity, plant stress and stomata closure points, hydraulic conductivity, root fraction within the saturated zone, and runoff coefficient. The model results were then evaluated against the actual data from 2006 and 2008, in order to perform an unbiased comparison. After calibration, the simulation was run using a randomly generated precipitation series, and the rainfall recycling factor for the system was adjusted until the 100-year average of annual precipitation matched the actual annual average for the site. The final parameter values are displayed on Table I. The

same calibration procedure was conducted for the Arizona site model, using the 2004/2006 data for calibration and 2005/2007 data for testing.

Multiple simulations were constructed in order to study the three disturbance scenarios. Although a wide range of investigations were possible using the model, we selected scenarios that would demonstrate the unique features of this modelling approach, particularly in examining the consequences of connectivity in these systems. As a result, ‘bottom-up’ connectivity with the atmosphere, as represented by recycling of ET, figures prominently in these scenarios. While ecohydrological models do not typically address it, the ET–atmospheric moisture–precipitation link could be important to savanna systems or during periods when the weather is not dominated by advecting storm fronts.

In order to illustrate the importance of the groundwater–soil–plant–atmosphere connection, the first set of disturbance scenario tests ‘lowered’ the groundwater tables on the phreatophytic sites (California and Arizona). Two methods were used: (1) the groundwater uptake from deep roots was ‘turned off’ while keeping the root distributions constant, in order to simulate immediate disconnection, (2) the root distribution was altered so that no deep roots were present, as might happen if vegetation was able to adapt to the absence of groundwater. We hypothesized (H1) that disconnection from groundwater would result in synergistically lower ET (i.e. ET rates that are lower than that accounted for by groundwater water) and that the effect would be exacerbated in sites with high land-atmosphere connectivity.

To assess the importance of the atmospheric feedback to system behaviour, the connection between ET and atmospheric moisture was removed by setting the recycling factor to zero. We wanted to determine if vegetation could rely only on atmospheric moisture conveyed into the area from outside the system. This disturbance scenario could be interpreted as gauging the impact of loss of connectivity in the land–atmosphere interactions. We hypothesized (H2) that severing the land-atmosphere

connection in the model would synergistically reduce both precipitation and ET; again, the effect would be exacerbated in sites with high land-atmosphere connectivity.

Finally, the third set of tests addressed the response of each savanna to a drought period. In these simulations, we examined the initial response of ET and precipitation to a drought, followed by the drought’s internal persistence after inputs to the system returned to normal. To eliminate consideration of natural variability, we created synthetic time series and perturbed them appropriately. For each site, a 365-day time series of atmospheric moisture imports, representative of a year with average precipitation, was selected from the randomly generated data. This time series was repeated for three initialization years to ensure the system was in equilibrium. In the fourth and fifth years, the same inputs were reduced by 50% to simulate the drought. In the sixth through tenth years, the normal time series was again used, to determine when the system would return to its initial state. We hypothesized (H3) that when multiyear droughts were simulated, the ecosystems would show progressively lower ET in successive years, with full recovery not occurring until several growing seasons after precipitation returns to normal, and that sites with stronger connections to the atmosphere and the groundwater would show a more muted response.

RESULTS

Model and measurement comparisons

Available data ranged from 4 years of daily precipitation, ET, and soil moisture at the California and Arizona sites to 2 years of daily soil moisture data at the Kenya Red Soil site and to no available data at the Kalahari (except one growing season of soil moisture data) and Kenya Black Cotton sites. This allowed us to test the model results from the Arizona and California sites using actual precipitation as a forcing and comparing the results to the measured values. These models were then

Table II. Comparison of modelled and measured data at the California site.

Average	Measured Value (2006, 2008)	Modeled Value 2 years Actual Precipitation	Modeled Value 10 years Random Precipitation
Precipitation (mm)	551	551 (0%)	563 (2%)
Runoff + recharge ^a + storage (mm)	157	179 (14%)	158 (1%)
Groundwater uptake (mm)	75.9	76.3 (0.4%)	67 (-12%)
$T_{grass} + E_{soil}$ (ET _{under} , mm)	187	178 (-5%)	209 (12%)
$T_{woody} + E_{can}$ (ET _{over} , mm)	208	195 (-6%)	203 (-2%)
ET _{total} (mm)	395	373 (-6%)	412 (5%)
Soil layer 1 water content (-)	0.227	0.216 (-5%)	0.232 (2%)
Soil layer 2 water content (-)	0.261	0.285 (9%)	0.292 (12%)
Ratio ET _{over} /ET _{total}	47%	52%	49%
Ratio ET _{total} /P	72%	68%	73%
Ratio RR/P	32%	55%	26%

^a Net recharge is the total yearly volume of water exiting the lower soil layer minus the groundwater uptake by vegetation.

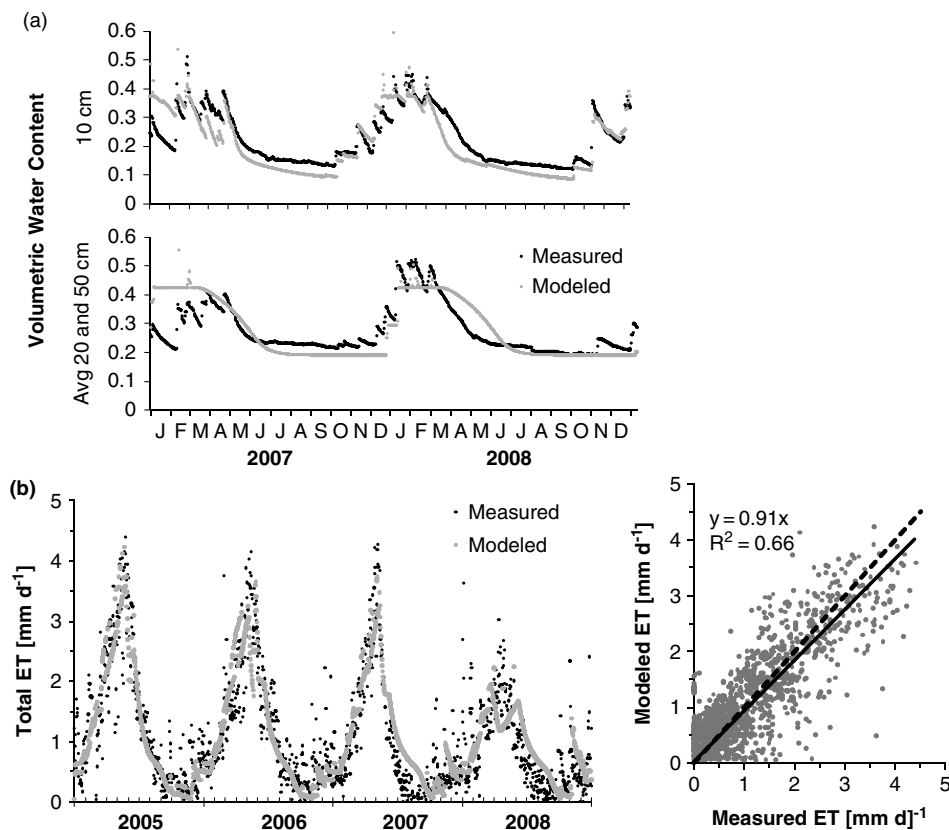


Figure 5. Comparison of (a) volumetric water content and (b) ET results from initial testing to data from the California oak savanna. In this test case, the model was driven by the actual precipitation data, rather than a random time series, to demonstrate its validity. The model was calibrated using the 2005 and 2007 data and tested against the 2006 and 2008 data.

calibrated based on a subset of data and tested against the remaining data, as described in the Methods section. At the Kenya Red site, daily soil moisture measurements were available, so the results found using randomly forced precipitation were compared statistically to the actual measurements.

California savanna. Modelled soil moisture and ET matched the annual data measured at the California oak savanna reasonably well, for simulations using the actual precipitation time series (Table II). The model slightly underpredicted the measured total ET (by 5–6%, or 22 mm), within the 5–20% error expected from the eddy covariance tower measurements (Wilson *et al.*, 2002). Predicted volumetric soil water content was within $0.011 \text{ m}^3 \text{ m}^{-3}$ for layer 1 and $0.024 \text{ m}^3 \text{ m}^{-3}$ for layer 2, both well within the anticipated error range for calibrated, capacitance style soil moisture probes ($\pm 0.03 \text{ m}^3 \text{ m}^{-3}$). The remaining portions of the water balance (runoff, recharge, and soil water storage) were summed into one value for comparison, as insufficient site data exists to resolve them. The modelled value of the combined terms was 179 mm, as compared to a measured value of 156 mm, for a difference of 22 mm (14%). The excess recharge, runoff, and storage were equivalent to the difference in total ET, indicating successful closure of the water balance equation.

The model was also able to accurately predict the seasonal and yearly trends in the time series of soil

moisture and ET (Figure 5a). The model effectively simulated the decline in soil moisture and ET due to low rainfall during 2008, the peak ET to within several days of the measured peaks, and spikes in grass and soil transpiration after winter rainfall events (Figure 5a). The date of grass senescence, inferred from soil moisture content, ranged from 25 May to 2 June (Day of Year (DOY) 145–153) in the model, while the date of grass ‘green-up’ varied from 22 October to 28 November (DOY 295–332). The observed ranges were wider, from 10 May 10 to 23 June (DOY 130–174) and from 23 October to 13 December (DOY 296–347). Measured and modelled dates were typically within 2 weeks of each other, again reflecting the models ability to exhibit interannual variability in grass ET and its ability to capture monthly to annual variations in soil moisture conditions.

As anticipated, the day-to-day variations inherent in the measured data were not captured (Figure 5b), because daily net radiation was not included as a model component. The plot of daily measured versus modelled ET (Figure 5b) indicated a positive correlation between the two ($r^2 = 0.67$), with the model slightly underpredicting ET ($\text{ET}_{\text{modelled}} = 0.91 \times \text{ET}_{\text{measured}}$). Soil moisture results displayed similar characteristics, with the model unable to reproduce fine, daily-to-weekly variations in moisture, particularly in the lower layer, but capturing the low frequency, seasonal and annual trends.

Table III. Comparison of modelled and measured data at the Arizona site.

Average	Measured value (2005, 2007)	Modelled value 2 years Actual precipitation	Modelled value 10 years Random precipitation
Precipitation (mm)	288	288 (0%)	360 (25%)
Runoff + recharge + storage (mm)	N/A	-272	-298
Groundwater uptake (mm)	281 ^a	281 (0%)	300 (7%)
$T_{grass} + E_{soil}$ (ET_{under} , mm)	N/A	223	294
$T_{woody} + E_{can}$ (ET_{over} , mm)	N/A	338	364
ET_{total} (mm)	569	561(-1%)	658 (16%)
Soil layer 1 water content (-)	0.0857	0.0821 (-4%)	0.0838 (-2%)
Soil layer 2 water content (-)	0.0953	0.0875 (-8%)	0.0817 (-14%)
Ratio ET_{over}/ET_{total}	N/A	60%	55%
Ratio ET_{total}/P	198%	195%	183%
Ratio RR/P	N/A	-89%	-79%

N/A, not applicable.
^a Assumed to equal $ET_{total} - P$.

Arizona savanna. Modelled soil moisture and ET matched the annual data measured at the Arizona shrubland site reasonably well, for simulations using the actual precipitation time series (Table III). For 2005 and 2007, the model predicted an average annual ET of 561 mm, 1% less than the measured value of 569 mm. Predicted volumetric soil water content was within $0.0036 \text{ m}^3 \text{ m}^{-3}$ for layer 1 and $0.0078 \text{ m}^3 \text{ m}^{-3}$ for layer 2, both within

the range of measurement error. Groundwater uptake was assumed to be equal to the difference between ET and precipitation, an average of 281 mm per year, and the model results matched this value. No data was available on the partitioning of ET between transpiration and soil evaporation or of the water balance between runoff, recharge, and storage at this site. However, Yopez *et al.* (2007) studied a nearby, denser riparian woodland with

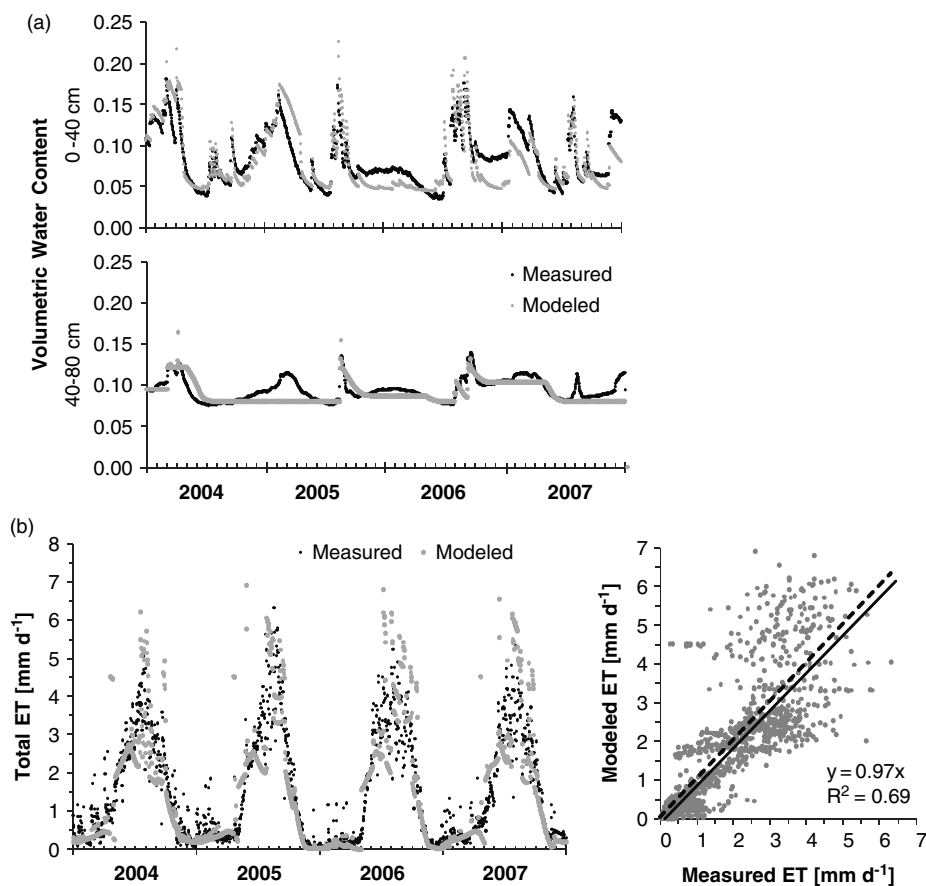


Figure 6. Comparison of (a) volumetric water content and (b) ET results from initial testing to data from the Arizona riparian shrubland. In this test case, the model was driven by the actual precipitation data, rather than a random time series, to demonstrate its validity. The model was calibrated using the 2004 and 2006 data and tested against the 2005 and 2007 data.

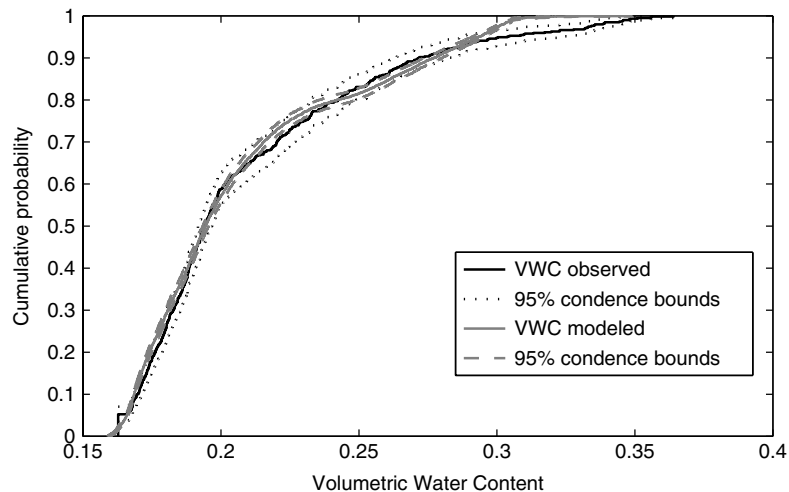


Figure 7. Comparison of modelled and observed volumetric water content under an *Acacia tortilis* collected over nearly a 2-year period at the Kenya Red Soil site, February 2007 through November 2008 (Franz, 2011). The comparison performs well over a wide range of the cumulative distribution function with model and/or observational errors only significantly affecting the distribution near rare, fully saturated conditions.

Table IV. Modelling results for site intercomparison.

Modelled average annual values	Tshane	Pandamatenga	Kenya Red	Kenya Black	Arizona	California
Precipitation (P)	294	661	500	556	360	563
Runoff (RO)	12.3	32.2	28.9	71.9	6.2	32.5
Net recharge (R)	9.2	22.2	0.1	0	-289	11
Groundwater uptake	0	0	0	0	300	66.9
$T_{\text{grass}} + E_{\text{soil}}$ (ET_{under})	158	157	232	183	294	210
$T_{\text{woody}} + E_{\text{can}}$ (ET_{over})	119	449	239	300	364	203
ET_{total}	277	606	471	483	658	413
Soil layer 1 water content	0.015	0.019	0.21	0.29	0.084	0.23
Soil layer 2 water content	0.021	0.018	0.17	0.26	0.082	0.29
Ratio $ET_{\text{over}}/ET_{\text{total}}$	43%	74%	51%	62%	55%	49%
Ratio ET_{total}/P	94%	92%	94%	87%	183%	73%
Ratio $(RO+R)/P$	7%	8%	6%	13%	-79%	27%

a fractional overstory cover of 0.75; they found a ratio of tree transpiration to total ET of 0.75. In comparison, the Arizona site in this study had a fractional coverage of 0.50 and a transpiration to ET ratio of 0.49, indicating that when scaled to account for differences in their canopies, the sites had very similar behaviour.

As with the California site, the model captured the seasonal trends in total ET well, but could not capture day-to-day variability due to its structure (Figure 6b). Modelled and measured values showed a positive correlation ($r^2 = 0.69$), with the model again slightly underpredicting ET ($ET_{\text{modelled}} = 0.97 \times ET_{\text{measured}}$). The modelled also described soil moisture in layer 1 well, predicting the response to individual rain events (Figure 6a). Some discrepancies were noted for layer 2, particularly during the beginning of 2005. In this case, layer 1 stayed wetter than indicated by the data, while layer 2 did not experience recharge.

Kenya Red Soil. Data at the Kenya Red Soil site were much more scarce than at the American savannas and were limited from monthly to annual precipitation

rates, annual runoff to precipitation ratios, and daily soil moisture values over the span of 2 years. When forced with a stochastic precipitation time series, the model found an average annual runoff fraction of 5.8%, close to the 1–5% range measured at the site (Franz, 2007).

Modelled daily volumetric water content values were statistically similar to those measured at the site (Franz, 2011). Figure 7 shows a comparison of their cumulative probability distributions for a 2 year period from February 2007 to November 2008. The model performs well over the range of soil moisture conditions, with some differences appearing on the fully saturated end of the continuum.

Simulations with 10-year stochastic rainfall forcing

Once the model was validated against the available data, 10-year simulations were conducted for each of the savanna sites, using randomly generated time series of atmospheric moisture inputs. Table IV shows the model results for each site, including the average annual values of each water balance component, the average soil water content, and the ratios of ET and runoff to precipitation.

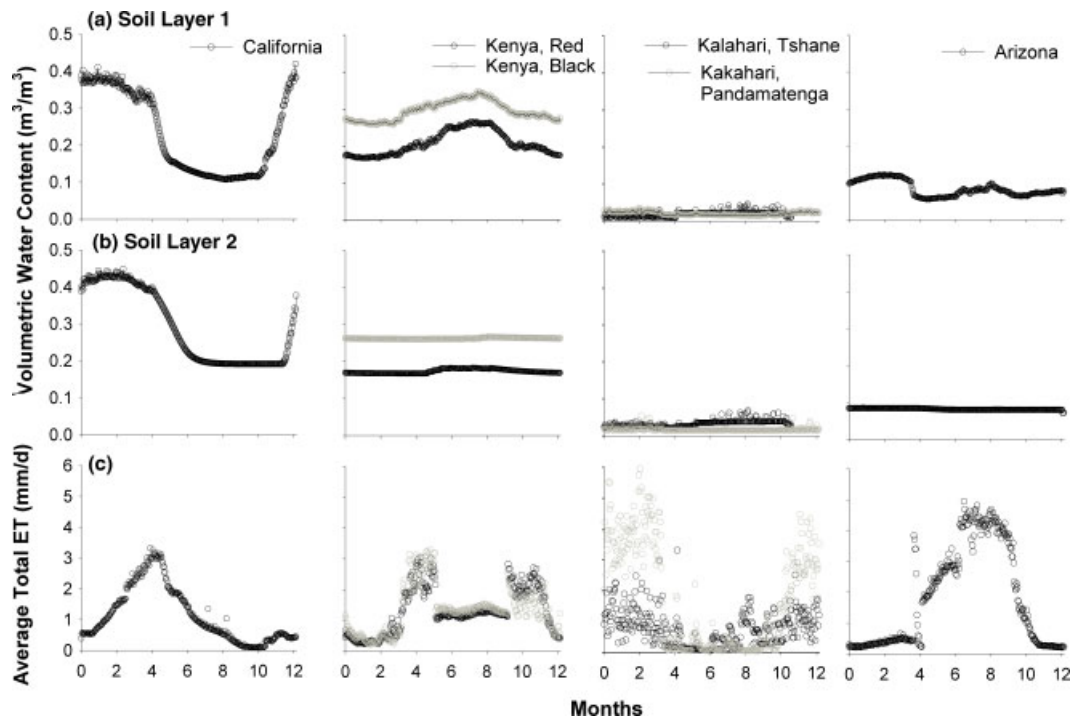


Figure 8. Modelling results for each of the sites. Values shown are averaged over the 10-year period and represent (a) soil moisture in layer 1, (b) soil moisture in layer 2, and (c) total ET.

Table V. Decrease in average annual values with no evapotranspiration recycling.

Water budget component	Tshane	Pandamatenga	Kenya Red	Kenya Black	Arizona	California
Initial f_r (%)	2	2	7	7	20	4
Initial $ET_{total} \times f_r$	5.5	12.1	33.0	33.8	132	17
Precipitation (mm)	5.6	12.0	32.9	34.0	132	16
Runoff (mm)	-0.03	0.6	1.8	3.3	2.1	0.5
Recharge (mm)	0.5	0.1	0.1	0.0	0.1	4.9
ET_{total} (mm)	5.0	11.4	31.0	30.4	129	11

Negative values indicate increase in water balance component.

Average daily values of soil moisture and ET are shown graphically in Figure 8.

Modelled average annual ET ranged from 277 mm at the Kalahari Tshane site to 658 mm at the Arizona site (Table IV). However, higher precipitation (P) did not necessarily correspond to higher ET; the highest modelled ET to P ratio, 183%, was found at the second driest site, in Arizona. Here, deeply rooted vegetation could access groundwater, which contributed an extra 300 mm per year to woody transpiration. This uptake was coupled with very low leakage from the bottom soil layer, resulting in a net negative value for recharge and runoff. In comparison, the lowest ET/P ratio, 73%, was found at the California site, which had precipitation out-of-sync with maximum ET demand.

Peak ET rates ranged from 3 to 6 mm day⁻¹ for the sites (Figure 8). The two sites along the Kalahari showed similar ET peak periods but different ET peak magnitude; the average ET values more than doubled at the wetter site (Figure 8, Table IV). The Kenya sites

had very similar seasonal patterns and peak rates, with two peaks in ET during the wet seasons from March to May (3.2 mm day⁻¹) and October to December (2.8 mm day⁻¹).

Given the diversity of precipitation time series generated, the 10-year simulations were able to capture the average annual values of the water balance components well. Using the randomly generated atmospheric inputs, the modelled values for precipitation, ET, and soil moisture at the California site matched the measured annual averages to within 2, 5, and 12%, respectively (Table II). At the Arizona site, predicted annual average values within 25, 16, and 14% of the data measured from 2004 to 2007 (Table III); however, all 4 years received below average rainfall. The average from the 10-year simulations (360 mm) compared much more favourably to the MAP (358 mm), with a 2% difference. All other sites had precipitation values within 6% of their annual averages.

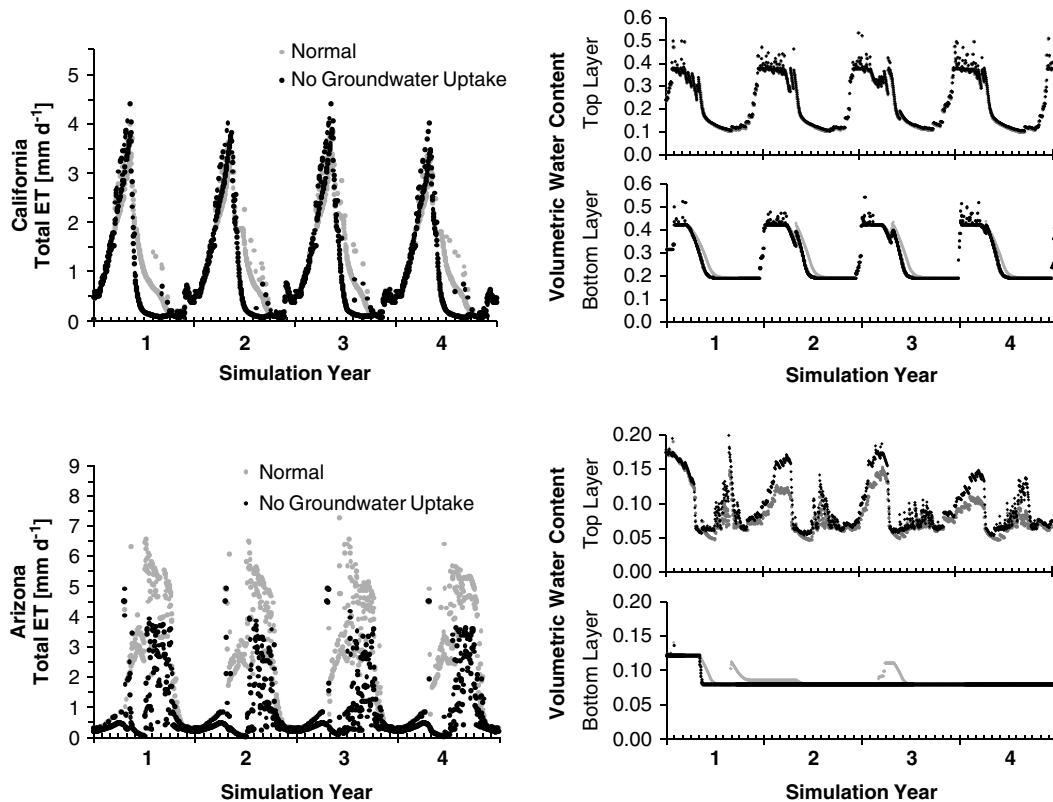


Figure 9. Impact of severing groundwater connection at phreatophytic sites: California (top) and Arizona (bottom). In both cases, the moisture in the lower soil layer is depleted more quickly or does not refill, while the total evapotranspiration is reduced, to near zero levels, during the drier months.

Disturbance scenario

For Disturbance Scenario 1, the fraction of roots into groundwater was set to zero for both the California and Arizona sites, simulating a sudden disconnection between the vegetation and the water table. The California and Arizona sites initially had groundwater uptake rates of 67 and 300 mm per year, respectively. When subjected to the complete, rapid disconnection of the roots from the groundwater source, the modelled rates were reduced, as anticipated, to zero (Figure 9). Tree transpiration was reduced correspondingly at the California savanna, by 68 mm, but the reduction was disproportionate at the Arizona site, which had a 319 mm reduction in tree transpiration and a 54 mm reduction in grass and soil ET. The higher degree of atmospheric connectivity at the Arizona site (with a 20% recycling ratio) led to a 74 mm reduction in precipitation, whereas the lower connectivity at the California site (4% recycling) yielded only a 3 mm decline in annual precipitation.

For Disturbance Scenario 2, the recycling ratio at each site was set to zero, to test the hypothesis that severing the land-atmosphere connection would synergistically reduce precipitation and ET. In all cases, changing the recycling factor to zero reduced the overall precipitation by an amount directly corresponding to the initial ET_{total} rate multiplied by the initial recycling factor (Table V). For instance, the Kenya Black Soil site had an initial $f_r = 7\%$ and $ET_{total} = 483$ mm, for a recycled precipitation amount of 34 mm; after reducing the recycling factor to zero, the precipitation was reduced by a corresponding

34 mm. The change in total ET did not have a one-to-one correspondence to rainfall reduction; it was consistently lesser than the change in precipitation (34 mm lower precipitation produced 30 mm lower ET). The remaining reductions were allocated to runoff (-3.3 mm).

In Disturbance Scenario 3, multiyear droughts were simulated for each site by reducing the fourth and fifth year atmospheric inputs by 50%. This reduction resulted in decrease of rainfall and ET at all four savanna ecosystems (Figure 10). The magnitudes in rainfall reduction at four regions varied from 39 to 51%, and the ET reductions varied from 11 to 50%, depending on the site. For all but the Kenya sites, precipitation was slightly (1–3%) lower after atmospheric inputs returned to normal, indicating only very short-term persistence of the drought. For the African sites, the reductions were identical (49% in the first year and 50% in the second), showing a linear relationship between reductions in atmospheric inputs, rainfall, and ET. The sites with groundwater uptake showed the lowest ET reductions, 11 and 21% in the first year and 19 and 20% in the second, for California and Arizona, respectively. Arizona experienced the full effect of the drought sooner due to its lower initial volumetric soil water storage (0.1 vs 0.4 $m^3 m^{-3}$).

DISCUSSION

The model accurately captured the ecohydrological processes of interest: ET from the soil, grass, and woody vegetation and soil moisture storage within the rooting

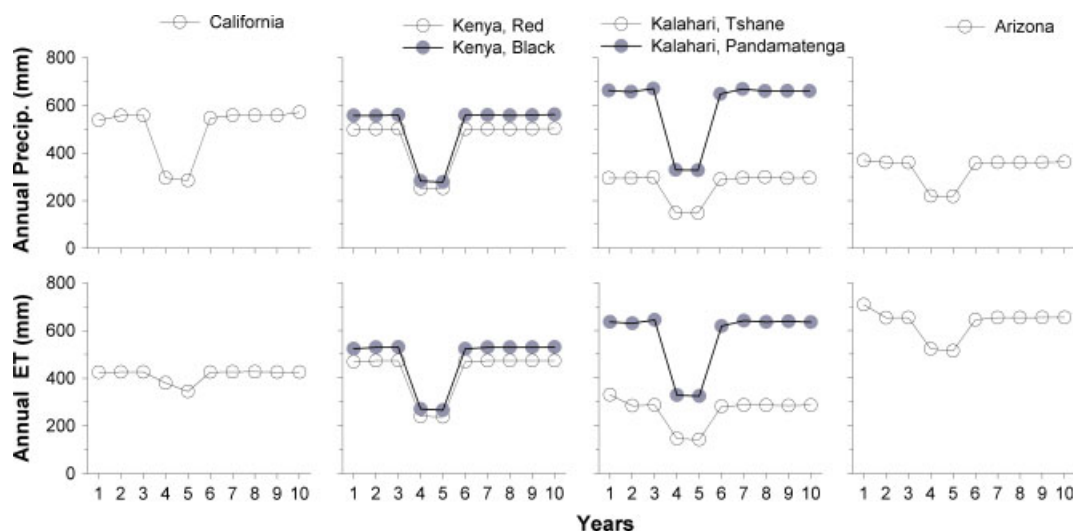


Figure 10. Impact of 2-year drought pulse on (a) evapotranspiration and (b) precipitation. To simulate a drought, the atmospheric imports of moisture were held constant at each site's average for years 1–3 and 6–10, while they were decreased by 50% in years 4 and 5, respectively. Most sites showed a larger decrease in ET for the second year of the drought (year 5), and several showed lowered ET for the year after imports returned to normal (year 6).

zone. The results demonstrate the model's ability to successfully depict both seasonal patterns and short-term, year-to-year variability. Monthly inputs in average evaporative demand and two soil moisture stocks provided sufficient temporal and spatial resolution to produce a nearly 1 : 1 ratio between measured and modelled ET data for the California and Arizona sites. However, because the model was not intended to predict ET on any given day, its application at a daily time-step resulted in a significant amount of scatter (Figures 5 and 6). Temporal patterns in mean soil moisture storage were well captured at all three tested sites. However, differences were most pronounced under two conditions: when soil was close to saturation and when water was being transferred between layers (Figures 6–8). This finding suggests that a daily time-step may be insufficient to fully capture infiltration processes and that a finer resolution of the soil layers (such as more than four depths), both in the model and field measurements, may result in a better fit.

The results also showed interannual variability in plant transpiration, which is a characteristic not normally revealed by ecohydrological models. At the California site, the length of the grass growing season notably differed depending on how long the wet season extended into the spring months. Both green-up and senescence occurred when the soil moisture time series crossed the grass stomatal closure point (S_{gc}); for example, senescence occurred when the actual soil moisture became lower than the value of S_{gc} . Both modelled and measured transpiration by woody vegetation showed less annual variability than that of grasses, due to woody plant access to deeper soil moisture and groundwater stores, which provided a more continuous water supply (Scott *et al.*, 2008).

Model simulations with stochastically generated time series illustrate the similarities and differences in the ecohydrology of the sites and provide a baseline for disturbance scenario testing. In general, the relative

timing of precipitation and evaporative demand was perhaps the largest influence on a site's ecohydrology, followed by soil texture. Comparing the modelled ET (Figure 8) with the rainfall inputs (Figure 2) and plots of E_{max} (Figure 3), three savanna paradigms emerge:

- (1) Constant evaporative demand but seasonal peak precipitation. These conditions occur at the Kenya sites given their equatorial location, which results in ET rates reflective of high water availability during the wet seasons (March to May and October to December). Here, grass is active during the two wet seasons, resulting in two annual peaks in ET. The more deeply rooted trees are active year round, which allows for continued, but suppressed, ET from June to September.
- (2) Peak evaporative demand and peak precipitation are synchronous. These conditions occur at the Kalahari sites, where the high demand summer months coincide with the wet season, resulting in both high ET and soil moisture. Grass and trees are both active year round, but their E_{max} values are significantly suppressed in the winter due to low demand.
- (3) Peak evaporative demand and peak precipitation are asynchronous for all or part of the growing season. These conditions are most apparent at the California site, which has a Mediterranean climate; here, the peak demand of summer occurs when precipitation is lowest, resulting in a late spring ET peak, quick depletion of soil moisture, and ET that is only sustained through groundwater uptake. The Arizona site, with its monsoonal climate, showed a more complex pattern with three distinctive phases: a low moisture/low demand period (November–April) where little ET occurred, a low moisture/high demand phase (May–early July) where groundwater provided for ET, and a high moisture/high demand phase in the monsoon season (July–October) where both

groundwater availability and elevated soil moisture combined to produce maximum ET rates.

As anticipated, soil texture strongly affected average soil moisture content, with lower soil moisture storage capacities in sandier soils (Kalahari and Arizona sites) (Figure 8). The effect on ET was more challenging to determine; the Kenya Black and Kenya Red sites were the only two paired sites in the study with similar climates but significantly different soil types and rooting depths. As a result, modelled ET was higher for the Black Soil site during the winter months (May through September) and lower during the spring months (October through January).

By testing three disturbance scenarios, we illustrated the potential uses of the SD approach and to assess the effects of vertical connectivity on processes in savanna ecosystems. H1 was partially supported by the results shown in Disturbance Scenario 1 (disconnection from the groundwater). At the Arizona and California sites, where woody vegetation accesses groundwater, disconnection from this source of water dropped ET to near zero for a portion of the growing season. However, the total change in annual ET was roughly proportional at the California site (67 mm lower uptake, 64 mm lower ET) and synergistic at the Arizona site (300 mm lower uptake, 373 mm lower ET). The effect was exacerbated at the site with higher rates land-atmosphere moisture recycling, as hypothesized, but the difference between the sites was also due to the relative differences in the timing and magnitude of the decrease. In the case of the Arizona site, 75 mm ($373 \text{ mm} \times 0.2$) of water was eliminated from the atmosphere during a time when precipitation events were relatively frequent (an average of 15 days between events). This contrasts with the California site, where 2.7 mm ($67 \text{ mm} \times 0.04$) was removed from circulation at a time of infrequent rainfall (100+ days between events). These results suggest that a higher degree of land-atmosphere connectivity is necessary to see the synergistic effect, or that processes that may lead to the effect are insufficiently modelled, e.g. die-off of vegetation due to inadequate water supplies. The model was not designed to consider the long-term consequences of this disconnection, as little to no data exists to inform it. As a result, trees which stopped transpiration early in the summer did not have changes in their physiology or behaviour in subsequent years, which is an unlikely outcome. Clearly, more data on tree mortality following groundwater disconnection, which is species or functional type specific, is needed.

H2 was not supported; severing the land-atmosphere connection in the model did not synergistically reduce both precipitation and ET, as shown by the results of Disturbance Scenario 2. When the recycling factor was reduced to zero, all sites responded with nearly proportionate reductions in precipitation and slightly lower reductions in ET. All sites displayed behaviour similar to that of the Kenya Black Soil site, described in the previous section. The components of the water balance were

not altered in proportionate ways, which demonstrates the model's ability to show negative feedback loops through the soil-plant-atmosphere continuum. In this instance, it shows the feedbacks between soil moisture, runoff, and ET. When runoff is created by a saturation excess mechanism, slightly lower soil moisture during wet periods may lead to more infiltration and lower runoff, creating a negative feedback that returns soil moisture levels closer to their original states. This action prevents the drier atmosphere and lower precipitation from having as dramatic of an impact on ET. Clearly, although, the extent to which this mechanism is protective is limited and strongly depends on runoff generation processes.

The results of Disturbance Scenario 3 partially supported H3—when multiyear droughts were simulated, the ecosystems showed progressively lower ET in successive years, with full recovery occurring between one to two growing seasons after precipitation returned to normal. Initial soil water storage and groundwater availability both reduced the initial ET response to drought. The effect was most prominent at the California site, where loamy soil texture and initially high (winter) storage conditions combined with groundwater uptake to provide a buffer for vegetation. For all the four savanna ecosystems, rainfall and ET values recovered to normal within the first 3 years after the drought. This recovery suggested that no long-term persistence in drought occurred, as soil storage stocks were quickly refilled.

The disturbance scenarios did not model the possibility of simultaneous system stressors causing permanent, catastrophic changes in system state. For example, one possible scenario: during a drought, groundwater levels are lowered considerably, creating conditions that resemble those found in both Disturbance Scenarios 1 and 3. Under these conditions, woody vegetation cannot survive, and the ecosystem begins to resemble a grassland rather than a savanna. Drought persistence could be much greater, as the system is knocked into a new stable equilibrium. In this case, key data, such as the relationship between groundwater levels and recharge and the mortality rates of trees under severe drought conditions, are missing. However, given the right inputs, the model could be used to simulate such catastrophic events.

CONCLUSIONS AND FUTURE WORK

This study demonstrated the utility and application of a dynamic systems model approach to understand ecohydrological connectivity in savannas. It revealed the system level consequences of disconnecting portions of the soil-plant-atmosphere continuum and changing the ecohydrology of savannah ecosystems. In landscapes that rely on groundwater uptake and recycle a moderate to high amount of ET as precipitation, disrupting either of these connections can create a positive feedback effect that reduces overall moisture availability. Model results suggested that savannas are more resistant to land-atmosphere disconnection than previously surmised and

implied that the ecohydrological effects of short-term droughts are also short-lived. Hydrologic mechanisms within the ecosystems, namely soil water storage, allow them to cope with short-term loss of groundwater connections or decreased connectivity with the atmosphere. However, thresholds may be reached with long-term loss of connectivity with the atmosphere (e.g. reductions in rainfall), as observed with the slower recovery of some systems from multiyear drought. These results highlight the need to further explore mechanisms associated with resilience and recovery from changes in water supply (either from below or above).

Tremendous opportunity exists for the further development and use of this type of modelling approach. This study only touched on the issue of patchiness in savannas. Future work will involve making the model more spatially detailed by (1) segregating the soil moisture components into true understory and overstory stocks and (2) creating a framework for representing patches of savanna vegetation by laterally linking multiple iterations of the model, with each iteration representing a different soil, vegetation, and terrain combination. These steps will be necessary to better understand the properties of the network–patchwork dynamic of connectivity, answer questions related to scaling fluxes in ecosystems, show the interaction between runoff and vegetation patches, remove the assumption of homogeneity across landscape scales, and allow for upscaling to regional levels. Such a model could help bridge the gap between simple dynamic ecosystem models and complex, but spatially explicit, land-atmosphere-subsurface codes such as PARFLOW.CLM (Maxwell and Miller, 2005).

To fully address questions of climate and land use change, we envision a model that ultimately incorporates the following processes: biogeochemical cycling, changes in phenology and physiology in response to system state changes, such as VPD-dependent ET, and dispersal and dieback of vegetation. Although they would increase the parameter requirements of the model, and thus the uncertainty, these additions could produce a new depth of complexity in the feedbacks observed and a richer understanding of savanna ecosystems.

ACKNOWLEDGEMENTS

The authors acknowledge the PIs of the following micrometeorological observation sites for use of their data in this research: Dennis Baldocchi (Tonzi Ranch Oak Savanna, US Department of Energy Terrestrial Carbon Project, Grant No DE-FG02-03ER63638), Russell Scott (USDA-ARS, San Pedro woody plant encroachment gradient), Kelly Caylor (Kenya sites, NSF OISE-0854708 and NSF CAREER award to K. Caylor EAR-847368, Princeton University, Grand Challenges, Walbridge Fund, and Technology for Developing Regions Fellowship), and Hank Shugart, Paolo D'Odorico, Greg Okin, and Stephen Macko (Kalahari Transect, NASA-IDS2, Grant

No NNG-04-GM71G). Lixin Wang greatly appreciates the teamwork and field assistance from Kelly Caylor, Todd Scanlon, Natalie Mladenov, Lydia Ries, and Thoralf Meyer. NCEP Reanalysis Derived data provided by the NOAA/OAR/ESRL PSD, Boulder, Colorado, USA, from their website at <http://www.esrl.noaa.gov/psd/>. We also thank two anonymous reviewers for their helpful and constructive feedback.

REFERENCES

- Ahmad S, Simonovic SP. 2000. System dynamics modeling of reservoir operations for flood management. *Journal of Computing in Civil Engineering* **14**(3): 190–198, DOI:10.1061/(ASCE)0887-3801(2000)14:3(190).
- Archer S. 1994. Woody plant encroachment into southwestern grasslands and savannas: rates, patterns and proximate causes. In *Ecological Implications of Livestock Herbivory in the West*, Vavra M, Laycock W, Pieper R (eds). Society for Range Management: Denver, CO; 13–68.
- Austin AT, Yahdjian L, Stark JM, Belnap J, Porporato A, Norton U, Ravetta DA, Schaeffer SM. 2004. Water pulses and biogeochemical cycles in arid and semiarid ecosystems. *Oecologia* **141**(2): 221–235, DOI:10.1007/s00442-004-1519-1.
- Baldocchi DD, Chen Q, Chen X, Ma S, Miller GR, Ryu Y, Xiao J, Wenk R. 2010. The dynamics of energy, water and carbon fluxes in a blue oak (*Quercus douglasii*) savanna in California, USA. In *Ecosystem Function in Global Savannas: Measurement and Modeling at Landscape to Global Scales*, Hill MJ, Hanan NP (eds). CRC Press: Boca Raton, FL; 135–151.
- Baldocchi DD, Xu LK, Kiang N. 2004. How plant functional-type, weather, seasonal drought, and soil physical properties alter water and energy fluxes of an oak-grass savanna and an annual grassland. *Agricultural and Forest Meteorology* **123**(1–2): 13–39, DOI:10.1016/j.agrformet.2003.11.006.
- Belnap J, Welter JR, Grimm NB, Barger N, Ludwig JA. 2005. Linkages between microbial and hydrologic processes in arid and semiarid watersheds. *Ecology* **86**(2): 298–307.
- Bhark EW, Small EE. 2003. Association between plant canopies and the spatial patterns of infiltration in shrubland and grassland of the Chihuahuan Desert, New Mexico. *Ecosystems* **6**(2): 185–196, DOI:10.1007/s10021-002-0210-9.
- Briske DD, Fuhlendor SD, Smeins EE. 2005. State-and-transition models, thresholds, and rangeland health: a synthesis of ecological concepts and perspectives. *Rangeland Ecology and Management* **58**(1): 1–10, DOI:10.2111/1551-5028(2005)58<1: SMTARH>2.0.CO;2.
- Calabrese JM, Fagan WF. 2004. A comparison-shopper's guide to connectivity metrics. *Frontiers in Ecology and the Environment* **2**(10): 529–536, DOI:10.1890/1540-9295(2004)002[0529: ACGTCM]2.0.CO;2.
- D'Odorico P, Porporato A. 2004. Preferential states in soil moisture and climate dynamics. *Proceedings of the National Academy of Sciences of the United States of America* **101**(24): 8848–8851.
- Dawson TE, Ehleringer JR. 1991. Streamside trees that do not use stream water. *Nature* **350**(6316): 335–337.
- Dirmeyer PA, Schlosser CA, Brubaker KL. 2009. Precipitation, recycling, and land memory: An integrated analysis. *Journal of Hydrometeorology* **10**(1): 278–288, DOI:10.1175/2008JHM1016.1.
- Dominguez F, Kumar P, Vivoni ER. 2008. Precipitation recycling variability and climatological stability—a study using NARR data. Part II: North American Monsoon Region. *Journal Of Climate* **21**(20): 5187–5203, DOI:10.1175/2008JCLI1760.1.
- Dunkerley DL. 2002. Infiltration rates and soil moisture in a groved mulga community near Alice Springs, arid central Australia: evidence for complex internal rainwater redistribution in a runoff-runon landscape. *Journal of Arid Environments* **51**(2): 199–219, DOI:10.1006/jare.2001.0941.
- Feddes RA, Kowalik PJ, Zaradny H. 1978. *Simulation of Field Water Use and Crop Yield*. Wiley: New York.
- Forrester JW. 2007. System dynamics—a personal view of the first fifty years. *System Dynamics Review* **23**(2–3): 345–358, DOI:10.1002/sdr.382.
- Franz T. 2007. *Ecohydrology of the Upper Ewaso River Basin, Kenya*. Princeton University: Princeton, NJ.

- Franz T. 2011. *Characterizing Dryland Surface Hydrological Dynamics Using Ecohydrological Modeling and Geophysical Observations*. Princeton University: Princeton, NJ.
- Franz TE, Caylor KK, Nordbotten JM, Rodríguez-Iturbe I, Celia MA. 2010. An ecohydrological approach to predicting regional woody species distribution patterns in dryland ecosystems. *Advances in Water Resources* **33**(2): 215–230.
- Franz TE, King EG, Caylor KK, Robinson DA. 2011. Coupling vegetation organization patterns to soil resource heterogeneity in a central Kenyan dryland using geophysical imagery. *Water Resources Research* doi:10.1029/2010WR010127.
- Haydon DT. 2000. Maximally stable model ecosystems can be highly connected. *Ecology* **81**(9): 2631–2636.
- Kalnay E, Kanamitsu M, Kistler R, Collins W, Deaven D, Gandin L, Iredell M, Saha S, White G, Woollen J, Zhu Y, Leetmaa A, Reynolds R, Chelliah M, Ebisuzaki W, Higgins W, Janowiak J, Mo KC, Ropelewski C, Wang J, Jenne R, Joseph D. 1996. The NCEP/NCAR 40-year reanalysis project. *Bulletin of the American Meteorological Society* **77**: 437–470, DOI:10.1175/1520-0477(1996)077<0437:TNYRP>2.0.CO;2.
- Khan S, Yufeng L, Ahmad A. 2009. Analysing complex behaviour of hydrological systems through a system dynamics approach. *Environmental Modelling and Software* **24**: 1363–1372, DOI:10.1016/j.envsoft.2007.06.006.
- Ludwig JA, Wilcox BP, Breshears DD, Tongway DJ, Imeson AC. 2005. Vegetation patches and runoff-erosion as interacting ecohydrological processes in semiarid landscapes. *Ecology* **86**(2): 288–297, DOI:10.1890/03-0569.
- Maxwell RM, Miller NL. 2005. Development of a coupled land surface and groundwater model. *Journal of Hydrometeorology* **6**(3): 233–247.
- Miller GR, Baldocchi DD, Law BE, Meyers T. 2007. An analysis of soil moisture dynamics using multi-year data from a network of micrometeorological observation sites. *Advances in Water Resources* **30**(5): 1065–1081, DOI:10.1016/j.advwatres.2006.10.002.
- Miller GR, Chen X, Baldocchi D, Rubin Y. 2010. Groundwater uptake by woody vegetation in a Mediterranean oak savanna. *Water Resources Research* **46**: W10503, DOI:10.1029/2009WR008902.
- Okin GS, D'Odorico P, Archer SR. 2009. Impact of feedbacks on Chihuahuan desert grasslands: transience and metastability. *Journal of Geophysical Research—Biogeosciences* **114**: G01004, DOI:10.1029/2008jg000833.
- Osmond B, Ananyev G, Berry J, Langdon C, Kolber Z, Lin GH, Monson R, Nichol C, Rascher U, Schurr U, Smith S, Yakir D. 2004. Changing the way we think about global change research: scaling up in experimental ecosystem science. *Global Change Biology* **10**(4): 393–407, DOI:10.1111/j.1529-8817.2003.00747.x.
- Peters DPC, Groffman PM, Nadelhoffer KJ, Grimm NB, Coffins SL, Michener WK, Huston MA. 2008. Living in an increasingly connected world: a framework for continental-scale environmental science. *Frontiers in Ecology and the Environment* **6**(5): 229–237, DOI:10.1890/070098.
- Peters DPC, Pielke RA, Bestelmeyer BT, Allen CD, Munson-McGee S, Havstad KM. 2004. Cross-scale interactions, nonlinearities, and forecasting catastrophic events. *Proceedings of the National Academy of Sciences of the United States of America* **101**(42): 15130–15135.
- Peters DPC, Yao J, Gosz JR. 2006. Woody plant invasion at a semi-arid/transition zone: importance of ecosystem type to colonization and patch expansion. *Journal of Vegetation Science* **17**(3): 389–396.
- Potts DL, Scott RL, Cable JM, Huxman TE, Williams DG. 2008. Sensitivity of mesquite shrubland CO₂ exchange to precipitation in contrasting landscape settings. *Ecology* **89**(10): 2900–2910, DOI:10.1890/07-1177.1.
- Ravi S, Breshears DD, Huxman TE, D'Odorico P. 2010. Land degradation in drylands: interactions among hydrologic-aolian erosion and vegetation dynamics. *Geomorphology* **116**(3–4): 236–245, DOI:10.1016/j.geomorph.2009.11.023.
- Reid KD, Wilcox BP, Breshears DD, MacDonald L. 1999. Runoff and erosion in a pinon-juniper woodland: influence of vegetation patches. *Soil Science Society of America Journal* **63**(6): 1869–1879.
- Richards JH, Caldwell MM. 1987. Hydraulic lift: substantial nocturnal water transport between soil layers by *Artemisia tridentata* roots. *Oecologia* **73**(4): 486–489, DOI:10.1007/bf00379405.
- Rodríguez-Iturbe I, Porporato A. 2004. *Ecohydrology of Water-controlled Ecosystems: Soil Moisture and Plant Dynamics*. Cambridge University Press: Cambridge, UK.
- Sala OE, Golluscio RA, Lauenroth WK, Soriano A. 1989. Resource partitioning between shrubs and grasses in the Patagonian steppe. *Oecologia* **81**(4): 501–505, DOI:10.1007/bf00378959.
- Saysel AK, Barlas Y. 2001. A dynamic model of salinization on irrigated lands. *Ecological Modelling* **139**(2–3): 177–199, DOI:10.1016/S0304-3800(01)00242-3.
- Schlesinger WH, Reynolds JF, Cunningham GL, Huenneke LF, Jarrell WM, Virginia RA, Whitford WG. 1990. Biological feedbacks in global desertification. *Science* **247**(4946): 1043–1048, DOI:10.1126/science.247.4946.1043.
- Scott RL, Cable WL, Huxman TE, Nagler PL, Hernandez M, Goodrich DC. 2008. Multiyear riparian evapotranspiration and groundwater use for a semiarid watershed. *Journal of Arid Environments* **72**(7): 1232–1246, DOI:10.1016/j.jaridenv.2008.01.001.
- Scott RL, Huxman TE, Williams DG, Goodrich DC. 2006. Ecohydrological impacts of woody-plant encroachment: seasonal patterns of water and carbon dioxide exchange within a semiarid riparian environment. *Global Change Biology* **12**(2): 311–324, DOI:10.1111/j.1365-2486.2005.01093.x.
- Sole RV, Montoya JM. 2001. Complexity and fragility in ecological networks. *Proceedings of the Royal Society B—Biological Sciences* **268**(1480): 2039–2045, DOI:10.1098/rspb/2001.1767.
- Tang GP, Bartlein PJ. 2008. Simulating the climatic effects on vegetation: approaches, issues and challenges. *Progress in Physical Geography* **32**(5): 543–556, DOI:10.1177/0309133308100443.
- Tischendorf L, Fahring L. 2000. On the usage and measurement of landscape connectivity. *Oikos* **90**(1): 7–19, DOI:10.1034/j.1600-0706.2000.900102.x.
- Trenberth KE. 1999. Atmospheric moisture recycling: role of advection and local evaporation. *Journal of Climate* **12**(5): 1368–1381.
- Trenberth KE, Dai A, Rasmussen RM, Parsons DB. 2003. The changing character of precipitation. *Bulletin of the American Meteorological Society* **84**(9): 1205–1217, DOI:10.1175/BAMS-84-9-1205.
- Van Auken OW. 2000. Shrub invasions of North American semiarid grasslands. *Annual Review of Ecology and Systematics* **31**: 197–215, DOI:10.1146/annurev.ecolsys.31.1.197.
- Ventana Systems. 2007a. *Vensim Reference Manual*. Ventana Systems: Harvard, MA.
- Ventana Systems. 2007b. *Vensim Version 5 User's Guide*. Ventana Systems: Harvard, MA.
- Wang L, D'Odorico P, Manzoni S, Porporato A, Macko S. 2009. Soil carbon and nitrogen dynamics in southern African savannas: the effect of vegetation-induced patch-scale heterogeneities and large scale rainfall gradients. *Climatic Change* **94**(1–2): 63–76, DOI:10.1007/s10584-009-9548-8.
- Wang L, D'Odorico P, Ringrose S, Coetzee S, Macko SA. 2007. Biogeochemistry of Kalahari sands. *Journal of Arid Environments* **71**(3): 259–279, DOI:10.1016/j.jaridenv.2007.03.016.
- Wang L, Zou C, O'Donnell F, Good S, Franz T, Miller GR, Caylor KK, Cable JM, Bond B. 2011. Characterizing ecohydrological and biogeochemical connectivity across multiple scales: a new conceptual framework. *Ecohydrology* this issue, DOI:10.1002/eco.187.
- Wiegand K, Saitz D, Ward D. 2006. A patch-dynamics approach to savanna dynamics and woody plant encroachment—insights from an arid savanna. *Perspectives in Plant Ecology, Evolution and Systematics* **7**(4): 229–242, DOI:10.1016/j.ppees.2005.10.001.
- Wilcox BP, Owens MK, Dugas WA, Ueckert DN, Hart CR. 2006. Shrubs, streamflow, and the paradox of scale. *Hydrological Processes* **20**(15): 3245–3259, DOI:10.1002/hyp.6330.
- Wilson K, Goldstein A, Falge E, Aubinet M, Baldocchi D, Berbigier P, Bernhofer C, Ceulemans R, Dolman H, Field C, Grelle A, Ibrom A, Law BE, Kowalski A, Meyers T, Moncrieff J, Monson R, Oechel W, Tenhunen J, Valentini R, Verma S. 2002. Energy balance closure at FLUXNET sites. *Agricultural and Forest Meteorology* **113**(1–4): 223–243, DOI:10.1016/S0168-1923(02)00109-0.
- Yepez E, Scott RL, Cable WL, Williams DG. 2007. Intra-seasonal variation in water and carbon dioxide flux components in a semiarid riparian woodland. *Ecosystems* **10**: 1100–1115, DOI:10.1007/s10021-007-9079-y.
- Young TP, Okello BD, Kinyua D, Palmer TM. 1998. KLEE: a long-term multi-species herbivore exclusion experiment in Laikipia, Kenya. *African Journal of Range and Forage Science* **14**(3): 94–102.
- Young TP, Patridge N, Macrae A. 1995. Long-term glades in Acacia bushland and their edge effects in Laikipia, Kenya. *Ecological Applications* **5**(1): 97–108, DOI:10.2307/1942055.

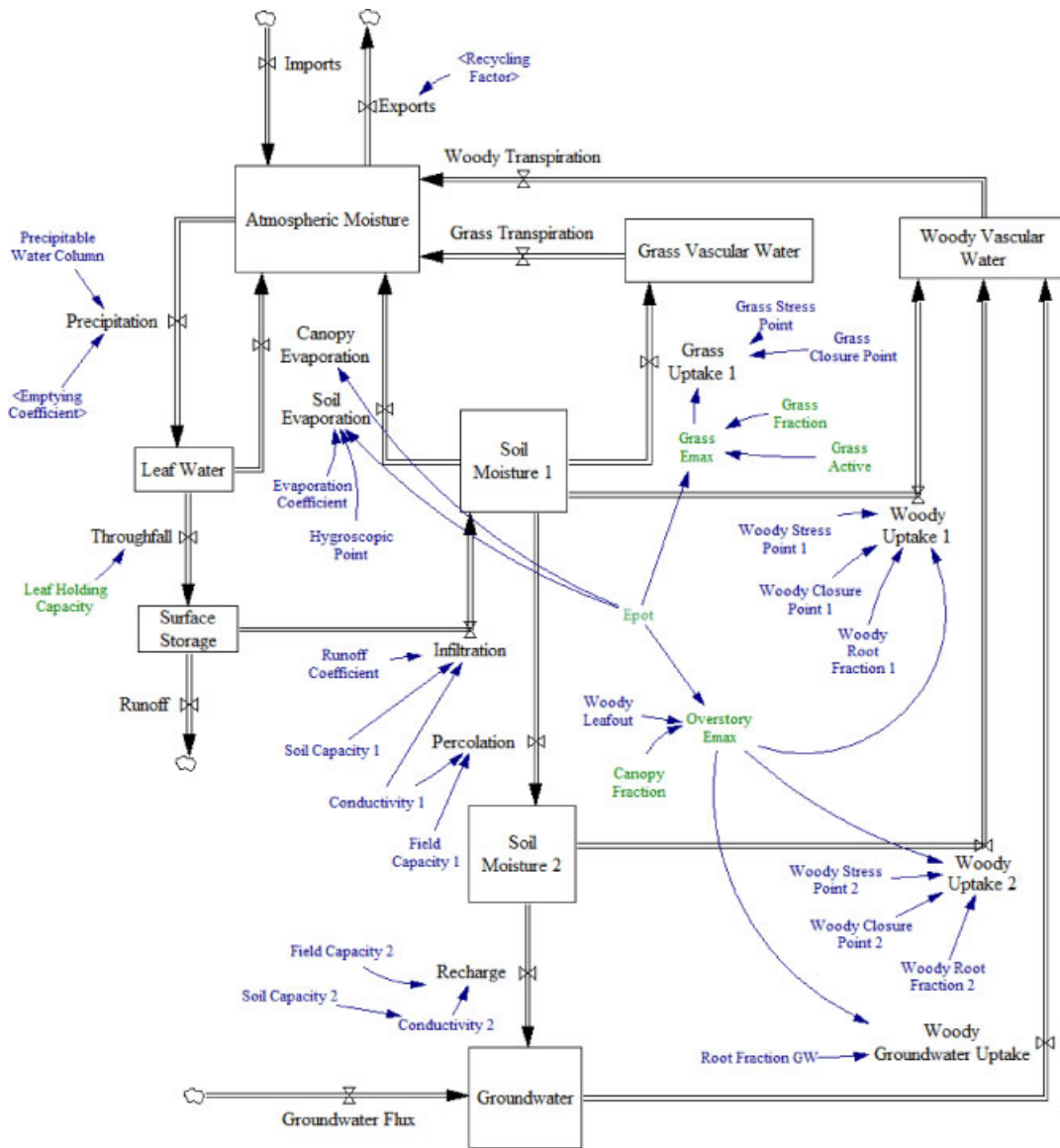


Figure A1. Diagram representing the implementation of the conceptual model (Figure 1) into a dynamic systems model, generated directly in the modelling software. Boxes indicate storage stocks while black arrows indicate flows. Blue arrows denote that a flow is dependent on a given parameter; parameters in dark blue have constant values and parameters in green are time-dependent.

APPENDIX: MODEL FORMULATION

SD models are represented by (1) stocks, or state variables, such as total available soil moisture, (2) flows, or flux rates, representing activities that add or deplete stocks, such as ET, and (3) connectors used to directionally link the variables, for instance, ET can only move water from the soil and vegetation surface to the atmosphere. Additionally, converters can be used to calculate intermediate variables, such as hydraulic conductivity at a certain soil moisture state. The structure of the model may be tested or verified using extreme conditions, such as drought, or behaviour sensitivity tests.

The model (Figure A1) developed in this study consists of a stock–flow loop connecting seven stocks: atmospheric moisture, water stored on the leaf surface, water stored on the ground surface, moisture in two layers of soil, groundwater, and plant tissue water. The differential equations describing the storage of water in each of

these stocks can be found in Table AI, along with notes describing the details of their implementation. The symbol *S* is used to denote the storage variable, with the subscript indicating the type (e.g. *S*_{soil1} for the first soil layer) and the units given as a depth of the water column (mm). Each of these stocks has a maximum storage capacity denoted by *S*_{stock,max}. For example, the maximum water stored in Soil layer 1 (*S*_{soil1,max}) is equal to the depth of that layer multiplied by its porosity. In this implementation, all *S*_{max} values are held constant; however, variable sizes may be appropriate for the plant tissue, leaf, and groundwater stocks, given sufficient data.

Flows of water in the model include (Table AII) imports and exports into the atmospheric column above a given area (*P*_{import}, *P*_{export}), precipitation (*P*), canopy throughfall (*F*), evaporation from the leaf surface (*E*_{can}), infiltration into the soil (*I*_{soil1}), percolation into the lower soil layer (*I*_{soil2}), recharge to groundwater (*I*_{soil3}), uptake

Table AI. Equations used to calculate storage in each stock.

Stock	Stock equations	Interpretation
Atmospheric moisture	$\frac{dS_{\text{atmos}}}{dt} = ET_{\text{total}} + P_{\text{import}} - P_{\text{export}} - P_{\text{event}}$	Precipitable water in the atmosphere, altered by randomly driven 'events' and by local ET.
Leaf surface	$\frac{dS_{\text{leaf}}}{dt} = P - E_{\text{can}} - F$	Water intercepted by leaf, evaporated from surface.
Plant tissues	$\frac{dS_{\text{grass}}}{dt} = U_{\text{grass},s1} + U_{\text{grass},s2} - T_{\text{grass}}$ $\frac{dS_{\text{woody}}}{dt} = U_{\text{woody},s1} + U_{\text{woody},s2} + U_{\text{woody},gw} - T_{\text{woody}}$	Water stored in plant tissues. Typically, this value is elastic over daily and seasonal timescales. For this analysis, S_{grass} and S_{woody} are held constant, but their inclusion in the model allows for future nutrient and carbon calculations.
Soil layer 1	$\frac{dS_{\text{soil1}}}{dt} = I_{\text{soil1}} - E_{\text{soil1}} - U_{\text{grass},s1} - U_{\text{woody},s1} - I_{\text{soil2}}$	Water stored near the soil surface, available for direct evaporation, plant uptake, and infiltration.
Soil layer 2	$\frac{dS_{\text{soil2}}}{dt} = I_{\text{soil2}} - U_{\text{grass},s2} - U_{\text{woody},s2} - I_{\text{soil3}}$	Water stored deeper in the soil, available for plant uptake, and groundwater recharge.
Surface water bodies	$\frac{dS_{\text{surf}}}{dt} = F - I_{\text{soil1}} - R$	Storage of water on the land surface, influenced by infiltration, runoff, and throughfall.
Groundwater aquifer	$\frac{dS_{\text{gw}}}{dt} = I_{\text{soil3}} - G$	Aquifer storage, as reflected by increasing and decreasing hydraulic heads.

The symbol S denotes storage in each stock, in millimetres, and t denotes time, in days. The following symbols represent flows, in millimetres per day: P , precipitation; T , transpiration; E , evaporation; U , root uptake; I , infiltration; F , throughfall; R , runoff; and G , groundwater flow. For a given time-step, storage values depend on the value from the previous time-step (or the initial conditions) and the flux into and out of the stock. The analysis presented here uses a 1-day time-step; however, the model could quickly be adapted for short periods. The subscript 'max' indicates the maximum storage capacity of the stock.

of water from woody vegetation and grass ($U_{\text{grass},\text{soil1}}$, $U_{\text{woody},\text{soil1}}$, $U_{\text{woody},\text{soil2}}$, $U_{\text{woody},\text{groundwater}}$), transpiration of water from woody vegetation and grass (T_{grass} , T_{woody}), and soil evaporation (E_{soil1}). These flow rates are calculated within the model at subdaily time-steps and vary depending on a combination of external parameters and on the state of the stock variables. A description of these flow rates and the processes they represent may be found below; they are also summarized in Table AII.

Precipitation is modelled stochastically, with time between both events and depth of events modelled as exponential variables (after Rodríguez-Iturbe and Porporato, 2004). A random time series of 'imports' into the atmosphere is generated using site-specific rainfall parameters. Precipitation may occur once the atmospheric stock of water becomes equal to or greater than the atmospheric saturation level, $S_{\text{atmos},\text{sat}}$. This value was found using the monthly average precipitable water, estimated by the NCEP/NCAR 40-year reanalysis project (Kalnay *et al.*, 1996), for the 2.5 × 2.5 degree latitude/longitude grid cell containing each site. The precipitation rate is deemed to be the difference between this value and the current level of water in the atmosphere ($S_{\text{atmos}} - S_{\text{atmos},\text{sat}}$) plus an additional amount between 0 and $S_{\text{atmos},\text{sat}}$, the value of which is randomly generated from an exponential distribution.

Exports from the atmosphere are modelled deterministically, with the rate of water loss equal to the ET rate modified by a recycling factor (f_r). Values for the recycling factor, for the African and California sites, were estimated from maps of the 'annual mean recycling ratio of the percentage of precipitation coming from

evaporation within a length scale of 1000 km' (Trenberth, 1999; Trenberth *et al.*, 2003). These maps were also developed using the NCEP reanalysis data on ET and the average horizontal flux of advected atmospheric moisture over a region. For the Arizona site, values from a study of the North American monsoon region were used instead (Dominguez *et al.*, 2008); these values are based on a grid with a 32-km length scale. Recycling ratios are known to vary by season, particularly in snow-covered and arid regions (Dirmeyer *et al.*, 2009). To simplify the modelling and analysis, we used the annual mean; however, variability could easily be added for future modelling tests. Use of these large-scale recycling ratios with small-scale eddy covariance data requires us to assume homogeneity in ET over the landscape.

Transpiration from the grass and woody vegetation was modelled using the common piecewise linear function (Feddes *et al.*, 1978; Rodríguez-Iturbe and Porporato, 2004), where the maximum possible transpiration (E_{max}) is a function of evaporative demand (E_{pot}) and fractional canopy coverage (f_{canopy}). In this model, when soil moisture (S_{soil1} , S_{soil2}) is above the plant stress point (S_{g^*} , S_{w^*}), transpiration is equal to E_{max} . As soil moisture declines past the stress point, plants begin to close their stomata, linearly reducing their transpiration rate. Once soil moisture reaches a critical point (S_{gc} , S_{wc}), the plants completely close their stomata and cease to transpire. In this model formulation, soil was divided into two layers, shallow and deep. To account for different soil moisture levels in each layer, the water uptake/transpiration from each layer was calculated by weighting E_{max} by its root fraction (e.g. $f_{\text{g},s1}$) and then calculating the actual

Table AII. Equations used to calculate flows to and from each stock.

Water flow	Flow equations	Interpretation
Total evapotranspiration	$ET_{total} = E_{can} + E_{soil} + T_{grass} + T_{woody}$	The total ET for the model is equal to the evaporation from the leaves and the soil plus the transpiration of the understory and overstory vegetation.
Evaporation from leaf surface	$E_{can} = \min(S_{leaf}, E_{pot})$	Over the course of 1 day, all water present on leaves evaporates, unless that rate is higher than the potential ET rate.
Soil evaporation	$E_{soil} = \begin{cases} E_{pot} \times f_{se}, & \text{if } S_{soil1} \geq S_h \\ 0, & \text{if } S_{soil1} < S_h \end{cases}$	Soil evaporation is a fraction of the potential ET.
Grass (understory) uptake	$U_{grass,si} = E_{max,grass}(1 - f_{canopy})f_{g,si} \times \begin{cases} 1, & \text{if } S_{soil,i} \geq S_{g^*,si} \\ \frac{(S_{soil,i} - S_{gc,si})}{(S_{g^*,si} - S_{gc,si})}, & \text{if } S_{gc,si} < S_{soil,i} < S_{g^*,si} \\ 0, & \text{if } S_{soil,i} \leq S_{gc,si} \end{cases}$	Transpiration is a piecewise linear function dynamically dependent on soil moisture status (after Rodriquez-Iturbe and Porporato, 2004). The subscripts <i>soil_i</i> and <i>si</i> represents the soil layer; here <i>i</i> = 1 to 2. E_{max} , which represents the average transpiration rate under well water conditions, changes depending on the season (see text and charts). The fractions $f_{w,mi}$ and $f_{g,si}$ represent the percentage of roots present in each soil layer, where $f_{w,s1} + f_{w,s2} + f_{w,g} = 1$ and $f_{g,s1} + f_{g,s2} = 1$. These values are constant in this implementation, but could be altered to change monthly if enough data are available. The fraction f_{canopy} indicates the fraction of woody vegetation canopy coverage.
Woody (overstory) uptake	$U_{woody,si} = E_{max,woody}f_{canopy}f_{w,si} \times \begin{cases} 1, & \text{if } S_{soil,i} \geq S_{w^*,si} \\ \frac{(S_{soil,i} - S_{wc,si})}{(S_{w^*,si} - S_{wc,si})}, & \text{if } S_{wc,si} < S_{soil,i} < S_{w^*,si} \\ 0, & \text{if } S_{soil,i} \leq S_{wc,si} \end{cases}$	
Uptake from groundwater	$U_{woody,g} = \begin{cases} E_{max,woody} \times f_{w,gw}, & \text{if } S_{soil1} \leq S_{w^*,s1} \text{ and } S_{soil2} \leq S_{w^*,s2} \\ 0, & \text{otherwise} \end{cases}$	The uptake rate of groundwater by woody vegetation, assumed to be equal to the well-watered ET, multiplied by the fraction of roots reaching the groundwater table. Uptake is assumed to occur only when the soil in both layers is below the stress point
Transpiration	$T_{grass} = U_{grass,s1} + U_{grass,s2}$ $T_{woody} = U_{woody,s1} + U_{woody,s2} + U_{woody,g}$	Understory transpiration equals the root water uptake of the grasses from both layers. Overstory transpiration equals the root water uptake of the woody vegetation, from both soil layers and from the saturated zone.
Moisture imports and exports	$P_{import} = \text{fxn}[\tau_{min}, \tau_{max}, \tau_{avg}, \text{fxn}(\alpha_{min}, \alpha_{max}, \alpha_{avg})]$ $P_{export} = ET_{total} \times (1 - f_{rc})$	Import of atmospheric moisture is a stochastic function based on the frequency (τ) and depth (α) of rain events observed at the sites. Their occurrence is based on a Poisson arrival process, and their depth is random and distributed exponentially. The export function includes a recycling factor, f_{rc} , which states what fraction of the evapotranspired water stays in the system.
Precipitation events	$P_{event} = \begin{cases} S_{atmos} - S_{atmos,sat} - S_{atmos,sat} \times f_p, & \text{if } S_{atmos} > S_{atmos,sat} \\ 0, & \text{if } S_{atmos} \leq S_{atmos,sat} \end{cases}$	Precipitation events occur when the total atmospheric storage of water is above the saturation point. The amount of precipitation can be higher than the amount needed to return to saturation, by a factor of f_p . This factor is a random value ranging from 0 to 1, generated by an exponential function.

Table AII. (Continued).

Water flow	Flow equations	Interpretation
Infiltration, percolation, and recharge	$I_{\text{soil1}} = \begin{cases} \min(K_{\text{soil1}}, S_{\text{surface}}, S_{\text{soil1,max}} - S_{\text{soil1}}), & \text{if } S_{\text{soil1}} < S_{\text{soil1,max}} \\ 0, & \text{if } S_{\text{soil1}} \geq S_{\text{soil1,max}} \end{cases}$ $I_{\text{soil2}} = \begin{cases} \max(K_{\text{soil1}}, S_{\text{soil1}} - S_{\text{fc,s1}}), & \text{if } S_{\text{fc,s1}} < S_{\text{soil1}} \\ 0, & \text{if } S_{\text{fc,s1}} \geq S_{\text{soil1}} \\ 0, & \text{if } S_{\text{soil2}} \geq S_{\text{soil2,max}} \end{cases}$ $I_{\text{gw}} = \begin{cases} \max(K_{\text{soil2}}, S_{\text{soil2}} - S_{\text{fc,s2}}), & \text{if } S_{\text{fc,s2}} < S_{\text{soil2}} \\ 0, & \text{if } S_{\text{fc,s2}} \geq S_{\text{soil2}} \end{cases}$	Water infiltrates from the surface to soil layer 1, percolates from soil layer 1 to 2, and recharges the groundwater from layer 2.
Runoff	$R = S_{\text{surf}} - I_{\text{soil1}}$	Runoff is the net difference between the amount that can be stored on the ground surface and the rate of infiltration into the top layer of soil.
Throughfall	$F = \begin{cases} P_{\text{event}} - S_{\text{leaf,max}}, & \text{if } P_{\text{event}} > S_{\text{leaf,max}} - S_{\text{leaf}} \\ P_{\text{event}}, & \text{otherwise} \end{cases}$	Throughfall is the difference between the amount of rain intercepted and the depth of the precipitation event.
Groundwater	$G = S_{\text{gw}} - S_{\text{gw,max}}$	In this model version, G is adjusted so that aquifer storage is constant. However, the framework is adaptable to allow for changing water table levels.

All flows are measured in depth per time, in the case of the analysis presented here, millimetres per day. When a flow is equal to a storage term, it is implied that this loss occurs over the span of 1 day, so that it is equivalent to a depth/time.

uptake from that layer ($U_{\text{g,s1}}$) based on the appropriate parameters ($S_{\text{g}^*,\text{soil1}}$, $S_{\text{gc,soil1}}$, $E_{\text{max,grass}}$). If vegetation can reach the underlying saturated zone, the woody plant uptake from groundwater ($U_{\text{w,g}}$) is equal to E_{max} multiplied by the fraction of roots present in this zone ($f_{\text{w,gw}}$).

Evaporation from the top soil layer was modelled in the same piecewise linear fashion as transpiration: a fraction (f_{sc}) of E_{pot} , constant when soil moisture is above the plant stomatal closure point and linearly decreasing until the soil hygroscopic point (S_{h}) is reached and evaporation drops to zero. Additionally, evaporation from the canopy surface on any given day is assumed to be equal to either E_{pot} or the amount of water stored on the leaf surface due to interception (S_{leaf}), whichever is lower.

Infiltration into the soil occurs when moisture content in the top layer is lesser than capacity ($S_{\text{soil1,max}}$) and a rainfall event occurs. The amount of water infiltrating in 1 day is equal to the remaining soil storage capacity ($S_{\text{soil1,max}} - S_{\text{soil1}}$) or the conductivity of the soil layer (K_{soil1}), whichever is smaller. When soil moisture exceeds field capacity ($S_{\text{fc,s1}}$, $S_{\text{fc,s2}}$), infiltration into the layer below occurs at a daily rate equal to the minimum

of the excess moisture in the leaking layer ($S_{\text{soil}} - S_{\text{soil,fc}}$) and hydraulic conductivity (K_{soil}).

Runoff occurs when the rate of water reaching the soil (F) is greater than the infiltration rate into the shallow soil layer; it can be due to either infiltration excess ($K_{\text{soil1}} < F$) or saturation excess ($S_{\text{soil1,max}} \leq S_{\text{soil1}}$). The actual value of F is equal to the precipitation measured above the canopy minus canopy and litter interception plus stemflow; however, no data on litter interception and stemflow are available for the modelled sites. Instead, we assume that the value of stemflow minus litter interception is negligible, making F functionally equal to the throughfall rate. The model includes a runoff coefficient (f_{run}) and a depression storage reservoir (S_{surf}) that can be adjusted to account for topographical or other physical factors not otherwise included. Since the current model is not spatially explicit and it is operated at ecosystem scale, the run-on process was not included.

Finally, the groundwater flow (G) is calculated such that groundwater storage remains constant; however, this can be adjusted according to the available data or to meet the desired modelling needs, such as changing groundwater availability.